Geophysical Prospecting **38**, 23–60, 1990

ELASTIC EXTRAPOLATION OF PRIMARY SEISMIC P- AND S-WAVES[1]

C. P. A. WAPENAAR and G. C. HAIMÉ[2]

ABSTRACT

WAPENAAR, C.P.A. and HAIMÉ, G.C. 1990. Elastic extrapolation of primary seismic P- and S-waves. *Geophysical Prospecting* **38**, 23–60.

The elastic Kirchhoff–Helmholtz integral expresses the components of the monochromatic displacement vector at any point A in terms of the displacement field and the stress field at any closed surface surrounding A. By introducing Green's functions for P- and S-waves, the elastic Kirchhoff–Helmholtz integral is modified such that it expresses either the P-wave or the S-wave at A in terms of the elastic wavefield at the closed surface. This modified elastic Kirchhoff–Helmholtz integral is transformed into one-way elastic Rayleigh-type integrals for forward extrapolation of downgoing and upgoing P- and S-waves. We also derive one-way elastic Rayleigh-type integrals for inverse extrapolation of downgoing and upgoing P- and S-waves. The one-way elastic extrapolation operators derived in this paper are the basis for a new prestack migration scheme for elastic data.

INTRODUCTION

Berkhout and Wapenaar (1988) proposed a new approach for processing of elastic seismic data which consists of the following steps (Fig. 1): (1) decomposition of the multi-component seismic data into one-way P^+-P^-. P^+-S^-, S^+-P^- and S^+-S^- data; (2) elimination of the surface related multiple reflections and conversions; (3) estimation of the elastic macro subsurface model from the P^+-P^- and S^+-S^- data; (4) modelling of forward and inverse one-way extrapolation operators for primary P- and S-waves; (5) shot record migration of the P^+-P^-, P^+-S^-, S^+-P^- and S^+-S^- data, yielding the subsurface reflectivity in terms of $R^+_{P\text{-}P}$, $R^+_{P\text{-}S}$, $R^+_{S\text{-}P}$ and $R^+_{S\text{-}S}$, optionally as a function of angle α; (6) elastic inversion for the detailed velocity and density information (c_p, c_s, ρ); (7) lithologic inversion for the rock and pore parameters.

The theory of the first two steps is discussed in detail by Wapenaar *et al.* (1990). It is interesting to note that the actual elastic migration (step 5) is not more

[1] Received December 1988, revision accepted May 1989.

[2] Delft University of Technology, Laboratory of Seismics and Acoustics, P.O. Box 5046, 2600 GA Delft, The Netherlands.

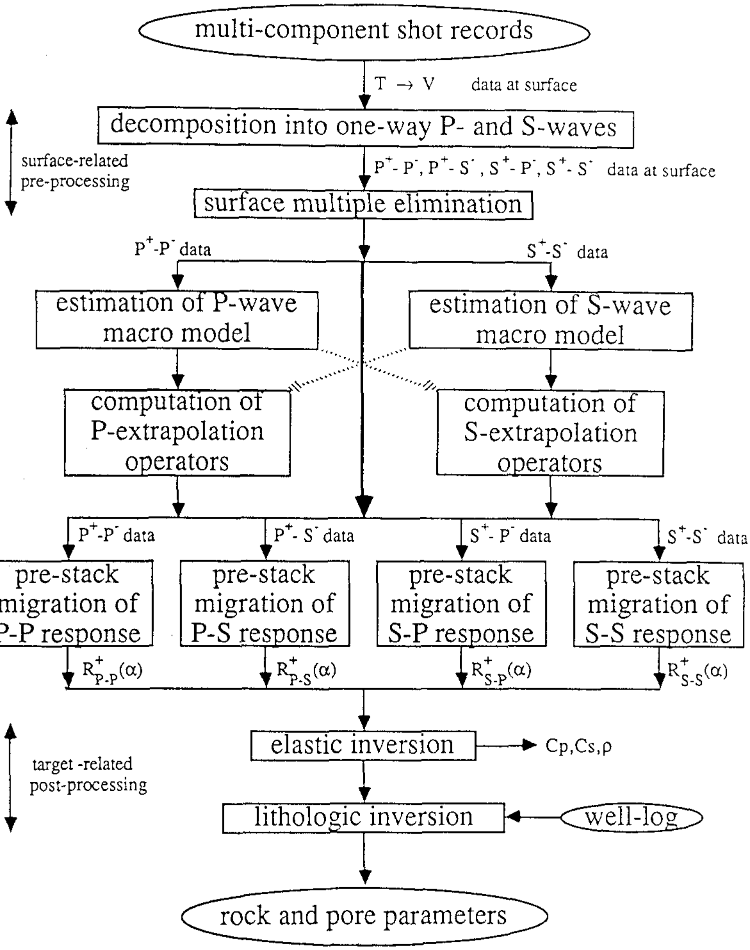

FIG. 1. Elastic seismic processing scheme.

complicated than acoustic shot record migration, e.g., migration of the P^+-S^- data can be accomplished with a standard shot record migration scheme in which we substitute extrapolation operators for downgoing P-waves and upgoing S-waves. Of course, the quality of the migrated sections will depend largely on the accuracy of the extrapolation operators which are modelled in step 4. This paper deals with the theory of the true amplitude extrapolation operators for primary P- and S-waves. After a brief review of the elastic Kirchhoff–Helmholtz integral for inhomogeneous anisotropic solids, we introduce the concept of elastic Green's functions for P- and S-waves. With these new Green's functions we derive elastic Kirchhoff–Helmholtz integrals for P- and S-waves. Next, following the same path as Berkhout and Wapenaar (1989, hereafter referred to as paper I), we derive one-way elastic Rayleigh integrals which are the basis for forward extrapolation operators for primary

P- and S-waves. Following the same path as Wapenaar *et al.* (1989, hereafter referred to as paper II), we also derive one-way elastic Rayleigh integrals with back-propagating Green's functions. These integrals are the basis for inverse extrapolation operators for primary P- and S-waves. They are well suited for application in shot record migration of P^+-P^-, P^+-S^-, S^+-P^- and S^+-S^- data (step 5 of the elastic processing scheme). We expect that this robust elastic one-way approach to seismic inversion will play a major role in the practice of seismic processing.

The Elastic Kirchhoff–Helmholtz Integral for Inhomogeneous Anisotropic Solids

We consider an inhomogeneous anisotropic solid, which is described by the space dependent mass density $\rho(\mathbf{r})$ and the stiffness tensor $\underset{\sim}{\mathbf{c}}(\mathbf{r})$, where $\mathbf{r}$ is a shorthand notation for the Cartesian coordinates (x, y, z). The components of the stiffness tensor are represented by $c_{ijkl}(\mathbf{r})$, where i (or j, k, l) $= 1, 2, 3$ stands for x, y, z, respectively. In this solid we consider a (sub)-volume V enclosed by a surface S with an outward pointing normal vector $\mathbf{n}$ (Fig. 2). Assuming that V is source free, then the space and frequency dependent elastic wavefield satisfies in V the linearized stress versus displacement relation (generalized Hooke's law)

$$\tau_{ij} - c_{ijkl}\,\partial_l U_k = 0 \tag{1a}$$

and the linearized equation of motion (generalized Newton's law)

$$\partial_j \tau_{ij} + \rho\omega^2 U_i = 0, \tag{1b}$$

(throughout this paper, the summation convention is assumed for repeated indices). Here U_i for $i = 1, 2, 3$ represents the three components of the displacement vector $\mathbf{U}(\mathbf{r}, \omega)$; τ_{ij} for $i = 1, 2, 3$ and $j = 1, 2, 3$ represents the nine components of the symmetric stress tensor $\underset{\sim}{\boldsymbol{\tau}}(\mathbf{r}, \omega)$; ω represents the radial frequency. Also in V we define Green's functions which satisfy the following equations:

$$\theta_{ij,m} - c_{ijkl}\,\partial_l G_{k,m} = 0 \tag{2a}$$

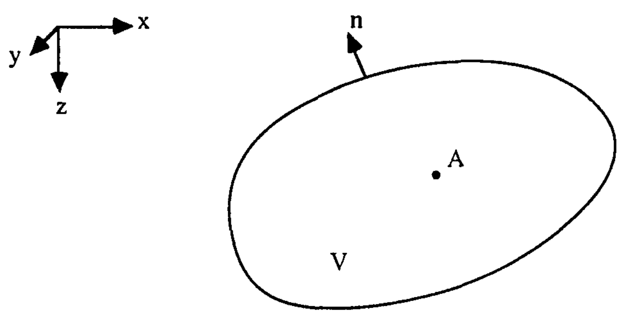

FIG. 2. Sub-volume V, enclosed by surface S, in an inhomogeneous anisotropic solid. V is assumed to be source free. The full elastic Kirchhoff–Helmholtz integral (4) states that the elastic wavefield at A in V can be computed when the elastic wave field is known on S.

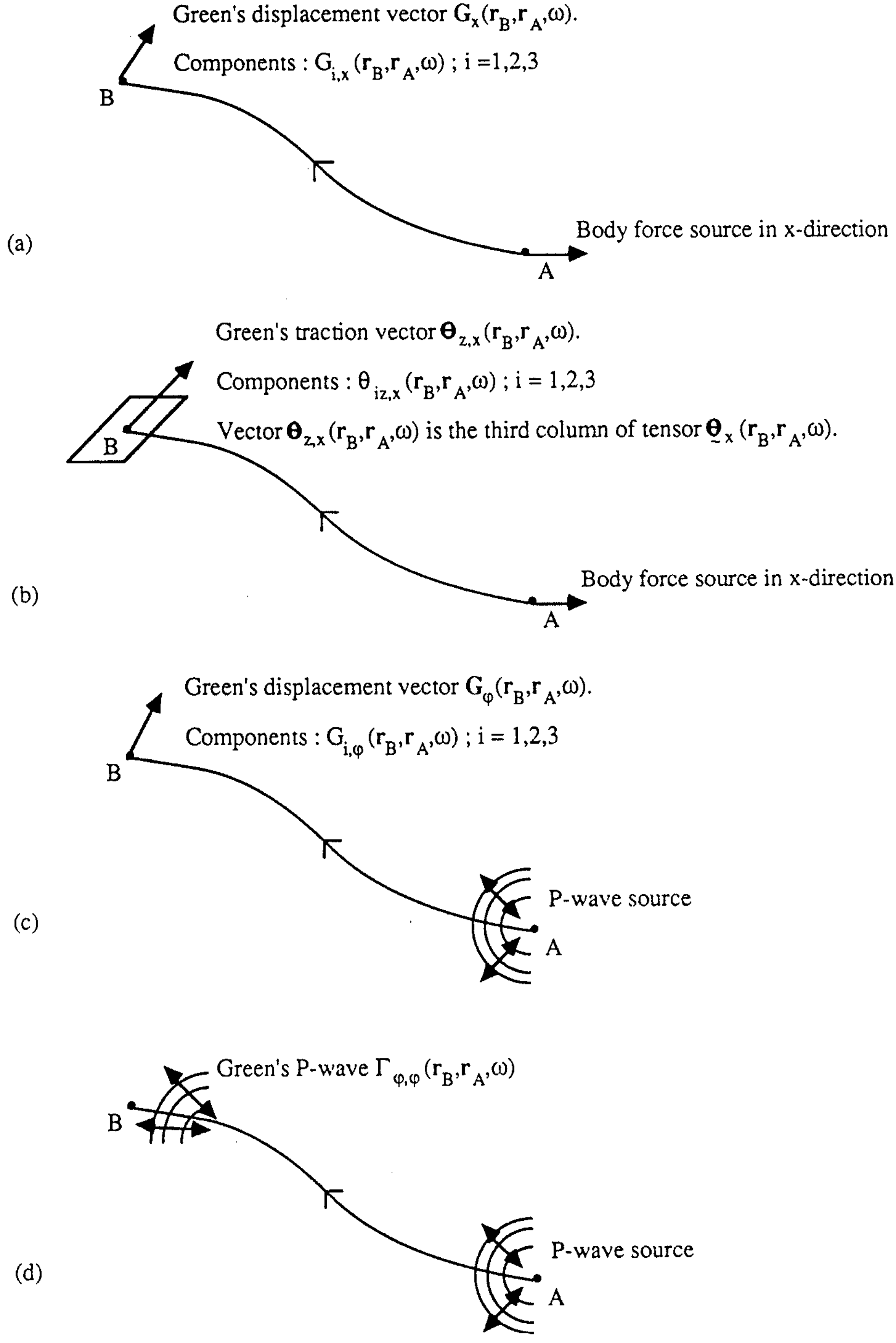

FIG. 3. Overview of elastic Green's function.

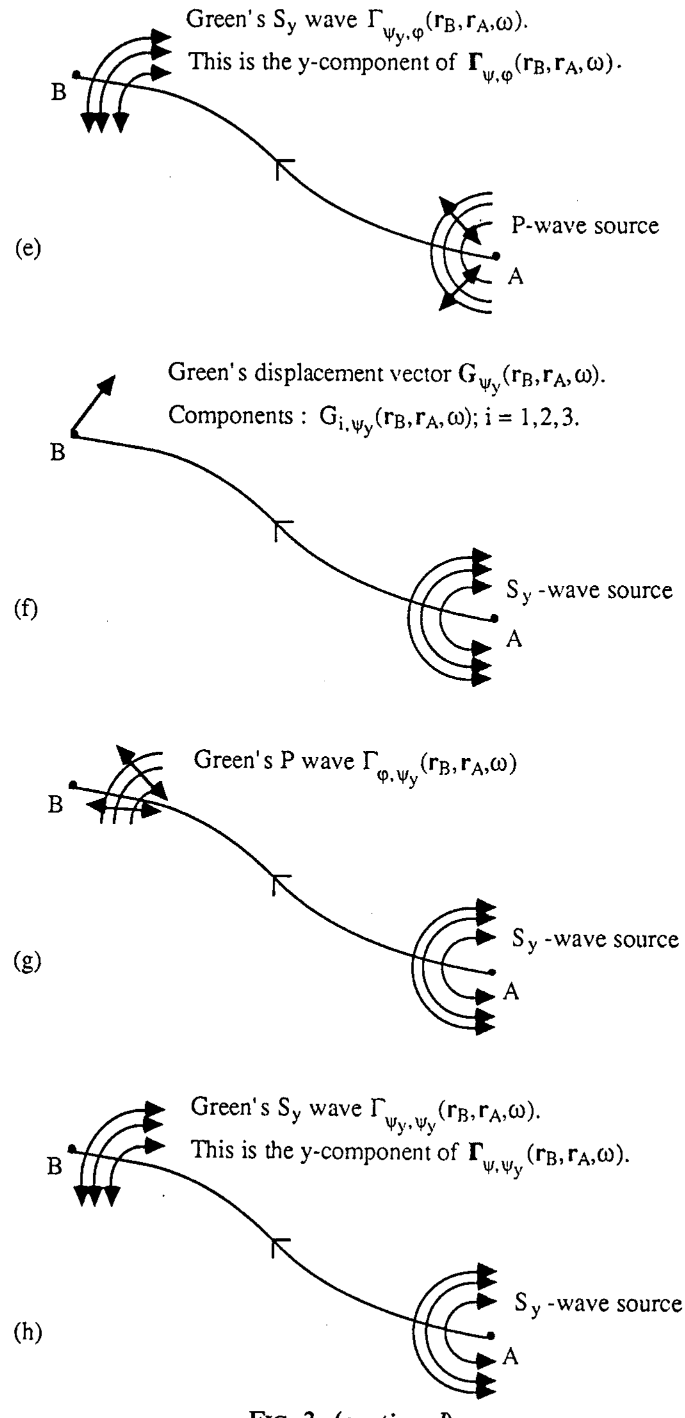

FIG. 3. *(continued)*

and

$$\partial_j \theta_{ij,m} + \rho\omega^2 G_{i,m} = -\delta_{im}\delta(\mathbf{r} - \mathbf{r}_A). \tag{2b}$$

Here δ_{im} is the Kronecker delta ($\delta_{im} = 1$ if $i = m$; $\delta_{im} = 0$ if $i \neq m$); $\mathbf{r}_A = (x_A, y_A, z_A)$ denotes the Cartesian coordinates of the Green's 'source point' A in V; $G_{i,m}$ for $i = 1, 2, 3$ represents the three components at 'observation point' $\mathbf{r}$ of the Green's displacement vector $\mathbf{G}_m(\mathbf{r}, \mathbf{r}_A, \omega)$; $\theta_{ij,m}$ for $i = 1, 2, 3$ and $j = 1, 2, 3$ represents the nine components at 'observation point' $\mathbf{r}$ of the Green's stress tensor $\underset{\sim}{\boldsymbol{\theta}}_m(\mathbf{r}, \mathbf{r}_A, \omega)$; finally, the subscript m, which may also take the values 1, 2, 3, refers to the direction of the unit body force at Green's 'source point' $\mathbf{r}_A$, (see Figs 3a and 3b). The Green's function satisfies the following reciprocity relation:

$$G_{i,m}(\mathbf{r}, \mathbf{r}_A, \omega) = G_{m,i}(\mathbf{r}_A, \mathbf{r}, \omega). \tag{2c}$$

When we apply the Gauss theorem

$$\int_V \nabla \cdot \mathbf{Q}_m \, dV = \oint_S \mathbf{Q}_m \cdot \mathbf{n} \, \mathrm{d}S \tag{3a}$$

to the vector function

$$\mathbf{Q}_m = \underset{\sim}{\boldsymbol{\tau}}\mathbf{G}_m - \underset{\sim}{\boldsymbol{\theta}}_m \mathbf{U}, \tag{3b}$$

where the components of $\mathbf{U}$, $\underset{\sim}{\boldsymbol{\tau}}$, $\mathbf{G}_m$, and $\underset{\sim}{\boldsymbol{\theta}}_m$ satisfy (1) and (2) in V, then we obtain the full elastic Kirchhoff–Helmholtz integral

$$U_m(\mathbf{r}_A, \omega) = \oint_S [\underset{\sim}{\boldsymbol{\tau}}(\mathbf{r}, \omega)\mathbf{G}_m(\mathbf{r}, \mathbf{r}_A, \omega) - \underset{\sim}{\boldsymbol{\theta}}_m(\mathbf{r}, \mathbf{r}_A, \omega)\mathbf{U}(\mathbf{r}, \omega)] \cdot \mathbf{n} \, \mathrm{d}S. \tag{4}$$

In the derivation, use was made of the symmetry properties $\tau_{ij} = \tau_{ji}$, $\theta_{ij,m} = \theta_{ji,m}$ and $c_{ijkl} = c_{klij}$. Representation theorem (4) states that the elastic wavefield at any point $\mathbf{r}_A$ in V can be calculated when the elastic wavefield in terms of $\mathbf{U}(\mathbf{r}, \omega)$ and $\underset{\sim}{\boldsymbol{\tau}}(\mathbf{r}, \omega)$ is known on S (see also De Hoop 1958; Burridge and Knopoff 1964; Aki and Richards 1980). Kuo and Dai (1984) use (4) as the starting point for an elastic wave migration scheme. They substitute Green's functions for homogeneous, isotropic layers and apply (4) recursively from layer interface to interface. In this paper we use (4) as the starting point for the derivation of forward and inverse one-way extrapolation operators for primary P- and S-waves. These operators are the basis for an elastic wave migration scheme for arbitrarily inhomogeneous anisotropic media (Berkhout and Wapenaar 1988).

Elastic Green's Functions for P- and S-Waves

After elimination of $\theta_{ij,m}$ from (2a) and (2b) we find that the components of the Green's displacement vector satisfy

$$\partial_j(c_{ijkl}\, \partial_l G_{k,m}) + \rho\omega^2 G_{i,m} = -\delta_{im}\delta(\mathbf{r} - \mathbf{r}_A). \tag{5}$$

Let us now assume that the solid medium is homogeneous and isotropic in a (infinitely) small region around the Green's source point $\mathbf{r}_A$. At $\mathbf{r}_A$ we define the constrained bulk compression modulus according to

$$K_c(\mathbf{r}_A) = \lambda(\mathbf{r}_A) + 2\mu(\mathbf{r}_A), \tag{6a}$$

where the Lamé coefficients λ and μ are related to the stiffness coefficients, according to

$$c_{ijkl}(\mathbf{r}_A) = \lambda(\mathbf{r}_A)\delta_{ij}\delta_{kl} + \mu(\mathbf{r}_A)(\delta_{ik}\delta_{jl} + \delta_{il}\delta_{jk}). \tag{6b}$$

We define an operator

$$-K_c(\mathbf{r}_A)\,\partial_m^A, \tag{7}$$

where ∂_m^A for $m = 1, 2, 3$ denotes differentiation with respect to the Green's source point coordinates x_A, y_A, z_A, respectively. By applying this operator to both sides of (5) we obtain

$$\partial_j(c_{ijkl}\,\partial_l G_{k,\varphi}) + \rho\omega^2 G_{i,\varphi} = -K_c(\mathbf{r}_A)\,\partial_i\delta(\mathbf{r} - \mathbf{r}_A), \tag{8a}$$

where we made use of the property

$$\partial_i^A\delta(\mathbf{r} - \mathbf{r}_A) = -\partial_i\delta(\mathbf{r} - \mathbf{r}_A),$$

and where

$$G_{i,\varphi}(\mathbf{r}, \mathbf{r}_A, \omega) \triangleq -K_c(\mathbf{r}_A)\,\partial_m^A G_{i,m}(\mathbf{r}, \mathbf{r}_A, \omega). \tag{8b}$$

$G_{i,\varphi}(\mathbf{r}, \mathbf{r}_A, \omega)$ for $i = 1, 2, 3$ represents the three components of a new Green's displacement vector $\mathbf{G}_\varphi(\mathbf{r}, \mathbf{r}_A, \omega)$. The right-hand side of (8a) is a source at $\mathbf{r}_A$ for P-waves (Wapenaar and Berkhout 1989). Hence, the subscript φ in $G_{i,\varphi}(\mathbf{r}, \mathbf{r}_A, \omega)$ refers to the P-wave character of the Green's source at $\mathbf{r}_A$ (see Fig. 3c). Of course, at observation point $\mathbf{r}$, this Green's function may consist of both P- and S-waves. Let us now assume that the solid medium is also homogeneous and isotropic in a (infinitely) small region around an observation point $\mathbf{r} = \mathbf{r}_B$. Then, in agreement with (A5a), we may define a Green's P-wave potential, according to

$$\Gamma_{\varphi,\varphi}(\mathbf{r}_B, \mathbf{r}_A, \omega) \triangleq -K_c(\mathbf{r}_B)\nabla^B \cdot \mathbf{G}_\varphi(\mathbf{r}_B, \mathbf{r}_A, \omega), \tag{8c}$$

or

$$\Gamma_{\varphi,\varphi}(\mathbf{r}_B, \mathbf{r}_A, \omega) \triangleq -K_c(\mathbf{r}_B)\,\partial_i^B \mathbf{G}_{i,\varphi}(\mathbf{r}_B, \mathbf{r}_A, \omega), \tag{8d}$$

where ∂_i^B for $i = 1, 2, 3$ denotes differentiation with respect to the Green's observation point coordinates x_B, y_B, z_B, respectively. In agreement with (A5b), we may also define a Green's S-wave potential, according to

$$\boldsymbol{\Gamma}_{\psi,\varphi}(\mathbf{r}_B, \mathbf{r}_A, \omega) \triangleq \mu(\mathbf{r}_B)\nabla^B \times \mathbf{G}_\varphi(\mathbf{r}_B, \mathbf{r}_A, \omega), \tag{8e}$$

or

$$\Gamma_{\psi_k,\varphi}(\mathbf{r}_B, \mathbf{r}_A, \omega) \triangleq -\mu(\mathbf{r}_B)\varepsilon_{kij}\,\partial_j^B G_{i,\varphi}(\mathbf{r}_B, \mathbf{r}_A, \omega), \tag{8f}$$

where ε_{kij} is the alternating tensor

$$\varepsilon_{kij} = 0 \text{ if any of } k, i, j \text{ are equal.} \tag{8g}$$

Otherwise

$$\varepsilon_{123} = \varepsilon_{312} = \varepsilon_{231} = -\varepsilon_{213} = -\varepsilon_{321} = -\varepsilon_{132} = 1, \tag{8h}$$

and hence by definition $\Gamma_{\psi_k,\varphi}$ represents the k-component of $\boldsymbol{\Gamma}_{\psi,\varphi}$.

In the following, the symbol Γ stands for Green's potential functions. The first subscript in $\Gamma_{\varphi,\varphi}(\mathbf{r}_B, \mathbf{r}_A, \omega)$ and $\Gamma_{\psi_k,\varphi}(\mathbf{r}_B, \mathbf{r}_A, \omega)$ refers to the wavetype at observation point $\mathbf{r}_B$; the second subscript refers to the wavetype at source point $\mathbf{r}_A$ (φ refers to P-waves, ψ_k refers to S_k-waves, polarized in the plane perpendicular to the k-axis; see Figs 3d and 3e).

So far we only considered modified Green's functions related to a P-wave source at $\mathbf{r}_A$. Next, we follow the same procedure for an S-wave source at $\mathbf{r}_A$. By applying the operator

$$-\mu(\mathbf{r}_A)\varepsilon_{hmn}\,\partial_n^A$$

to both sides of equation (5) we obtain

$$\partial_j(c_{ijkl}\,\partial_l G_{k,\psi_h}) + \rho\omega^2 G_{i,\psi_h} = -\mu(\mathbf{r}_A)\varepsilon_{hin}\,\partial_n \delta(\mathbf{r} - \mathbf{r}_A), \tag{9a}$$

where

$$G_{i,\psi_h}(\mathbf{r}, \mathbf{r}_A, \omega) \triangleq -\mu(\mathbf{r}_A)\varepsilon_{hmn}\,\partial_n^A G_{i,m}(\mathbf{r}, \mathbf{r}_A, \omega). \tag{9b}$$

$G_{i,\psi_h}(\mathbf{r}, \mathbf{r}_A, \omega)$ for $i = 1, 2, 3$ represents the three components of a new Green's displacement vector $\mathbf{G}_{\psi_h}(\mathbf{r}, \mathbf{r}_A, \omega)$. The right-hand side of (9a) is a source at $\mathbf{r}_A$ for S_h-waves, polarized in the plane perpendicular to the h-axis (Wapenaar and Berkhout 1989). Hence, the subscript ψ_h refers to the S_h-wave character of the Green's source at $\mathbf{r}_A$ (see Fig. 3f). At the observation point $\mathbf{r} = \mathbf{r}_B$ this Green's function may consist of both P- and S-waves. In agreement with (A5a) we define a Green's P-wave potential according to

$$\Gamma_{\varphi,\psi_h}(\mathbf{r}_B, \mathbf{r}_A, \omega) \triangleq -K_c(\mathbf{r}_B)\nabla^B \cdot \mathbf{G}_{\psi_h}(\mathbf{r}_B, \mathbf{r}_A, \omega), \tag{9c}$$

or

$$\Gamma_{\varphi,\psi_h}(\mathbf{r}_B, \mathbf{r}_A, \omega) \triangleq -K_c(\mathbf{r}_B)\,\partial_i^B G_{i,\psi_h}(\mathbf{r}_B, \mathbf{r}_A, \omega) \tag{9d}$$

(see Fig. 3g). In agreement with (A5b) we define a Green's S-wave potential, according to

$$\boldsymbol{\Gamma}_{\psi,\psi_h}(\mathbf{r}_B, \mathbf{r}_A, \omega) \triangleq \mu(\mathbf{r}_B)\nabla^B \times \mathbf{G}_{\psi_h}(\mathbf{r}_B, \mathbf{r}_A, \omega), \tag{9e}$$

or

$$\Gamma_{\psi_k,\psi_h}(\mathbf{r}_B, \mathbf{r}_A, \omega) \triangleq -\mu(\mathbf{r}_B)\varepsilon_{kij}\,\partial_j^B G_{i,\psi_h}(\mathbf{r}_B, \mathbf{r}_A, \omega), \tag{9f}$$

where Γ_{ψ_k,ψ_h} represents by definition the k-component of $\boldsymbol{\Gamma}_{\psi,\psi_h}$ (see Fig. 3h). From reciprocity relation (2c) and from definitions (8b), (8d), (8f), (9b), (9d) and (9f), the following reciprocity relations can be derived:

$$\Gamma_{\varphi,\varphi}(\mathbf{r}_B, \mathbf{r}_A, \omega) = \Gamma_{\varphi,\varphi}(\mathbf{r}_A, \mathbf{r}_B, \omega), \tag{10a}$$

$$\Gamma_{\psi_k,\psi_h}(\mathbf{r}_B, \mathbf{r}_A, \omega) = \Gamma_{\psi_h,\psi_k}(\mathbf{r}_A, \mathbf{r}_B, \omega), \tag{10b}$$

and

$$\Gamma_{\psi_k,\varphi}(\mathbf{r}_B, \mathbf{r}_A, \omega) = \Gamma_{\varphi,\psi_k}(\mathbf{r}_A, \mathbf{r}_B, \omega). \tag{10c}$$

Note that these reciprocity relations hold for arbitrarily inhomogeneous anisotropic elastic media. The only assumption is that the medium is locally homogeneous and isotropic at $\mathbf{r}_A$ and $\mathbf{r}_B$. In the following sections we make extensive use of these Green's functions for P- and S-waves.

Elastic Kirchhoff–Helmholtz Integrals for P- and S-Waves

Kirchhoff–Helmholtz integral (4) expresses the displacement U_m at $\mathbf{r}_A$ in terms of the elastic wavefield on S. We now derive Kirchhoff–Helmholtz integrals which express the P-wave potential or the S-wave potential at $\mathbf{r}_A$ in terms of the elastic wavefield on S. Again we assume that the medium is homogeneous and isotropic in a (infinitely) small region around $\mathbf{r}_A$. Hence, in agreement with (A5a) we can define a P-wave potential at $\mathbf{r}_A$, according to

$$\Phi(\mathbf{r}_A, \omega) \triangleq -K_c(\mathbf{r}_A)\nabla^A \cdot \mathbf{U}(\mathbf{r}_A, \omega), \tag{11a}$$

or

$$\Phi(\mathbf{r}_A, \omega) \triangleq -K_c(\mathbf{r}_A)\, \partial_m^A U_m(\mathbf{r}_A, \omega). \tag{11b}$$

By substituting Kirchhoff–Helmholtz integral (4) and changing the order of integration (over $S(\mathbf{r})$) and differentiation (at $\mathbf{r}_A$), we obtain

$$\Phi(\mathbf{r}_A, \omega) = \oint_S [\underset{\sim}{\tau}(\mathbf{r}, \omega)\mathbf{G}_\varphi(\mathbf{r}, \mathbf{r}_A, \omega) - \underset{\sim}{\Theta}_\varphi(\mathbf{r}, \mathbf{r}_A, \omega)\mathbf{U}(\mathbf{r}, \omega)] \cdot \mathbf{n}\, \mathrm{d}S, \tag{12a}$$

where

$$\mathbf{G}_\varphi(\mathbf{r}, \mathbf{r}_A, \omega) = -K_c(\mathbf{r}_A)\, \partial_m^A \mathbf{G}_m(\mathbf{r}, \mathbf{r}_A, \omega) \tag{12b}$$

and

$$\underset{\sim}{\Theta}_\varphi(\mathbf{r}, \mathbf{r}_A, \omega) = -K_c(\mathbf{r}_A)\, \partial_m^A \underset{\sim}{\Theta}_m(\mathbf{r}, \mathbf{r}_A, \omega). \tag{12c}$$

Kirchhoff–Helmholtz integral (12a) states that the P-wave potential at $\mathbf{r}_A$ can be computed from the elastic wavefield on S with the aid of Green's functions that have a P-wave source at $\mathbf{r}_A$. The components of $\mathbf{G}_\varphi$ were already defined in (8b), so in practice they are found by solving (8a) rather than by solving (2) for $m = 1, 2, 3$ and applying (12b). Subsequently, the components of $\underset{\sim}{\boldsymbol{\theta}}_\varphi$ are found by applying

$$\theta_{ij,\varphi} = c_{ijkl}\,\partial_l G_{k,\varphi} \tag{12d}$$

on S.

Next, in agreement with (A5b) we define an S-wave potential at $\mathbf{r}_A$, according to

$$\boldsymbol{\Psi}(\mathbf{r}_A, \omega) \triangleq \mu(\mathbf{r}_A)\boldsymbol{\nabla}^A \times \mathbf{U}(\mathbf{r}_A, \omega), \tag{13a}$$

or

$$\Psi_h(\mathbf{r}_A, \omega) \triangleq -\mu(\mathbf{r}_A)\varepsilon_{hmn}\,\partial_n^A U_m(\mathbf{r}_A, \omega), \tag{13b}$$

where Ψ_h represents by definition the h-component of $\boldsymbol{\Psi}$. By substituting Kirchhoff–Helmholtz integral (4) and changing the order of integration and differentiation we obtain

$$\Psi_h(\mathbf{r}_A, \omega) = \oint_S [\underset{\sim}{\boldsymbol{\tau}}(\mathbf{r}_A, \omega)\mathbf{G}_{\psi_h}(\mathbf{r}, \mathbf{r}_A, \omega) - \underset{\sim}{\boldsymbol{\theta}}_{\psi_h}(\mathbf{r}, \mathbf{r}_A, \omega)\mathbf{U}(\mathbf{r}, \omega)] \cdot \mathbf{n}\, \mathrm{d}S. \tag{14a}$$

This Kirchhoff–Helmholtz integral states that the S_h-wave potential at $\mathbf{r}_A$ can be computed from the elastic wavefield on S with the aid of Green's functions that have an S_h-wave source at $\mathbf{r}_A$. The components of $\mathbf{G}_{\psi_h}$ are defined by (9b), so in practice they are found by solving (9a). Subsequently, the components of $\underset{\sim}{\boldsymbol{\theta}}_{\psi_h}$ are found by applying

$$\theta_{ij,\psi_h} = c_{ijkl}\,\partial_l G_{k,\psi_h} \tag{14b}$$

on S.

Kirchhoff–Helmholtz integrals (4), (12a) and (14a) can be summarized as

$$\Omega(\mathbf{r}_A, \omega) = \oint_S [\underset{\sim}{\boldsymbol{\tau}}\mathbf{G}_\Omega - \underset{\sim}{\boldsymbol{\theta}}_\Omega \mathbf{U}] \cdot \mathbf{n}\, \mathrm{d}S, \tag{15}$$

where $\Omega(\mathbf{r}_A, \omega)$ stands for $U_m(\mathbf{r}_A, \omega)$, or $\Phi(\mathbf{r}_A, \omega)$ or $\Psi_h(\mathbf{r}_A, \omega)$ and where $\mathbf{G}_\Omega$, $\underset{\sim}{\boldsymbol{\theta}}_\Omega$ stand for $\mathbf{G}_m$, $\underset{\sim}{\boldsymbol{\theta}}_m$ or $\mathbf{G}_\varphi$, $\underset{\sim}{\boldsymbol{\theta}}_\varphi$ or $\mathbf{G}_{\psi_h}$, $\underset{\sim}{\boldsymbol{\theta}}_{\psi_h}$, respectively.

One-way Versions of the Elastic Kirchhoff–Helmholtz and Rayleigh Integrals

Consider the geometry of Fig. 4. Closed surface S consists of a horizontal flat surface S_0 at $z = z_0$ and a hemisphere S_1 in the lower half space $z \geq z_0$, with midpoint A and radius R. Assuming that the sources are situated in the upper half space $z < z_0$, then the contribution of the Kirchhoff–Helmholtz integral over S_1 to the wavefield in A vanishes if R goes to infinity, (Sommerfield radiation conditions, Pao and Varatharajulu 1976). Hence, for this situation (15) may be replaced by

$$\Omega(\mathbf{r}_A, \omega) = \iint_{-\infty}^{+\infty} [\boldsymbol{\theta}_{z,\Omega} \cdot \mathbf{U} - \mathbf{G}_\Omega \cdot \boldsymbol{\tau}_z]_{z_0}\, \mathrm{d}x\, \mathrm{d}y, \tag{16}$$

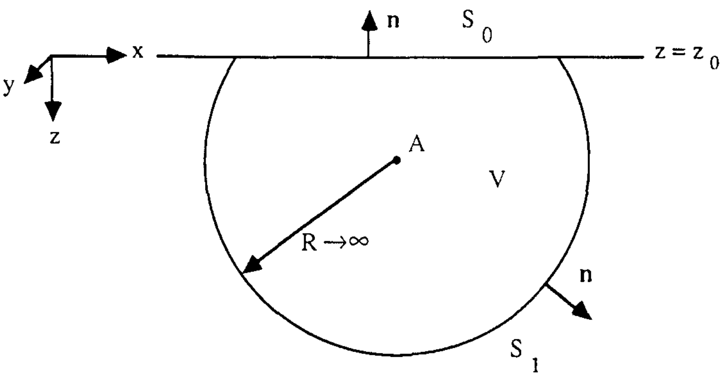

FIG. 4. Configuration for which the closed surface integral (15) may be replaced by the open surface integral (16). The lower half space is assumed to be source free.

where we used the fact that $\mathbf{n}$ on S_0 is a unit vector in the negative z-direction. The tractions $\boldsymbol{\tau}_z$ and $\boldsymbol{\theta}_{z,\Omega}$ represent the third column of the tensor $\underset{\sim}{\tau}$ and $\underset{\sim}{\theta}_{\Omega}$, respectively. In the following we assume that the medium is homogeneous and isotropic (described by λ, μ and ρ) in a (infinitely) thin region around the surface z_0. So in this region the wavefield can be separated into downgoing and upgoing waves. In addition, for the Green's functions we choose a homogeneous and isotropic upper half space. This choice is justified, because in the derivation of the Kirchhoff–Helmholtz integral we only considered the medium inside S, which is the lower half space. With this choice, the Green's functions at z_0 represent purely upgoing waves. Equation (16) can now be rewritten as

$$\Omega(\mathbf{r}_A, \omega) = \iint_{-\infty}^{+\infty} [\boldsymbol{\theta}^-_{z,\Omega} \cdot (\mathbf{U}^+ + \mathbf{U}^-) - \mathbf{G}^-_{\Omega} \cdot (\boldsymbol{\tau}^+_z + \boldsymbol{\tau}^-_z)]_{z_0} \,\mathrm{d}x\,\mathrm{d}y. \tag{17}$$

Here the superscripts $+$ and $-$ denote downward and upward propagation, respectively. In agreement with (A2) we define P- and S-wave potentials at z_0 for the wavefield and for the Green's functions, according to

$$[\mathbf{U}^{\pm}(\mathbf{r}, \omega)]_{z_0} \triangleq \frac{1}{\rho\omega^2}[\nabla\Phi^{\pm} + \nabla \times \boldsymbol{\Psi}^{\pm}]_{z_0}, \tag{18a}$$

(see Fig. 5a) and

$$[\mathbf{G}^-_{\Omega}(\mathbf{r}, \mathbf{r}_A, \omega)]_{z_0} \triangleq \frac{1}{\rho\omega^2}[\nabla\Gamma^-_{\varphi,\Omega} + \nabla \times \boldsymbol{\Gamma}^-_{\psi,\Omega}]_{z_0}. \tag{18b}$$

(see Fig. 5b). It is shown in Appendix B that by applying the one-way wave equations for the P- and S-wave potentials at z_0, the elastic Kirchhoff–Helmholtz integral (17) can be transformed to

$$\Omega(\mathbf{r}_A, \omega) = -2\iint_{-\infty}^{+\infty} \frac{1}{\rho\omega^2}\left[\Gamma^-_{\varphi,\Omega}\frac{\partial\Phi^+}{\partial z} + \boldsymbol{\Gamma}^-_{\psi,\Omega} \cdot \frac{\partial\boldsymbol{\Psi}^+}{\partial z}\right]_{z0} \mathrm{d}x\,\mathrm{d}y, \tag{19a}$$

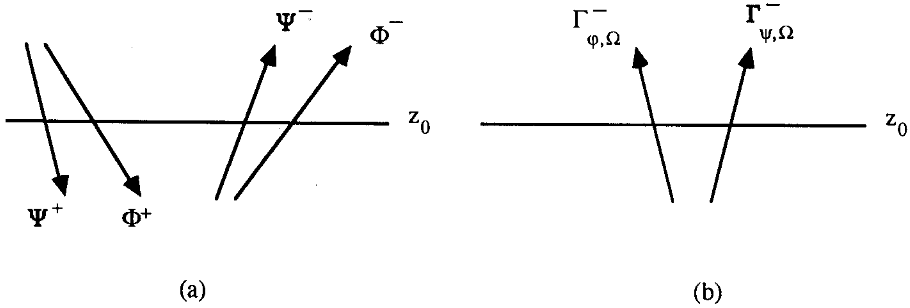

FIG. 5. Downgoing and upgoing P- and S-wave potentials at $z = z_0$. (a) Potentials for the elastic wavefield. (b) Potentials for the Green's functions.

or alternatively to

$$\Omega(\mathbf{r}_A, \omega) = 2 \iint_{-\infty}^{+\infty} \frac{1}{\rho\omega^2} \left[\frac{\partial \Gamma^-_{\varphi,\Omega}}{\partial z} \Phi^+ + \frac{\partial \boldsymbol{\Gamma}^-_{\psi,\Omega}}{\partial z} \cdot \boldsymbol{\Psi}^+ \right]_{z0} \mathrm{d}x\, \mathrm{d}y. \tag{19b}$$

Note the high degree of similarity of these equations with the one-way acoustic Rayleigh integrals that were derived in paper I. Equation (19a) represents the one-way elastic Rayleigh I integral; equation (19b) represents the one-way elastic Rayleigh II integral. Note that in both integrals only the downgoing P-wave interacts with an upgoing Green's P-wave, and the downgoing S-wave interacts with an upgoing Green's S-wave. No interaction occurs between the P-wave and the Green's S-wave or between the S-wave and the Green's P-wave. Finally, note that for the configuration of Fig. 4, equations (19a) and (19b) are exact; the only assumption is that the medium is locally homogeneous and isotropic at z_0 and at $\mathbf{r}_A$.

ONE-WAY ELASTIC RAYLEIGH INTEGRALS FOR P- AND S-WAVES

Depending on the choice of the source for the Green's functions, Ω in (19a) and (19b) can represent either U_m for $m = 1, 2, 3$ or Φ or Ψ_h. We consider the latter two cases. If the Green's functions have a P-wave source at $\mathbf{r}_A$, then Ω represents the P-wave potential at $\mathbf{r}_A$. For instance, for (19b) we may now write

$$\Phi(\mathbf{r}_A, \omega) = 2 \iint_{-\infty}^{+\infty} \frac{1}{\rho\omega^2} \left[\frac{\partial \Gamma^-_{\varphi\varphi}}{\partial z} \Phi^+ + \frac{\partial \boldsymbol{\Gamma}^-_{\psi,\varphi}}{\partial z} \cdot \boldsymbol{\Psi}^+ \right]_{z0} \mathrm{d}x\, \mathrm{d}y. \tag{20a}$$

On the other hand, if the Green's functions have an S_h-wave source at $\mathbf{r}_A$, then Ω represents the S_h-wave potential at $\mathbf{r}_A$. For (19b) we may now write

$$\Psi_h(\mathbf{r}_A, \omega) = 2 \iint_{-\infty}^{+\infty} \frac{1}{\rho\omega^2} \left[\frac{\partial \Gamma^-_{\varphi,\psi_h}}{\partial z} \Phi^+ + \frac{\partial \boldsymbol{\Gamma}^-_{\psi,\psi_h}}{\partial z} \cdot \boldsymbol{\Psi}^+ \right]_{z0} \mathrm{d}x\, \mathrm{d}y. \tag{20b}$$

Here $\Gamma^-_{\varphi,\varphi}$, $\boldsymbol{\Gamma}^-_{\psi,\varphi}$, $\Gamma^-_{\varphi,\psi_h}$ and $\boldsymbol{\Gamma}^-_{\psi,\psi_h}$ represent upgoing Green's potentials for P- and S-waves. Equation (20a) represents a one-way full elastic Rayleigh II integral for the computation of the P-wave potential in the subsurface. If we assume that the sources in the upper half-space generate mainly *P*-waves, then $|\boldsymbol{\Psi}^+|$ at z_0 will be small compared with $|\Phi^+|$. The Green's source at $\mathbf{r}_A$ is a P-wave source, so also $|\boldsymbol{\Gamma}^-_{\psi,\varphi}|$ at z_0 will be small compared with $|\Gamma^-_{\varphi,\varphi}|$. Hence, the magnitude of the product $(\partial\boldsymbol{\Gamma}^-_{\psi,\varphi}/\partial z)\cdot\boldsymbol{\Psi}^+$ is proportional to multiply converted waves, so it is two orders lower than the magnitude of $(\partial\Gamma^-_{\varphi,\varphi}/\partial z)\Phi^+$ at z_0. In other words, for P-wave sources in the upper half space, (20a) may be approximated by

$$\Phi(\mathbf{r}_A, \omega) \approx 2 \iint_{-\infty}^{+\infty} \frac{1}{\rho\omega^2} \left[\frac{\partial \Gamma^-_{\varphi,\varphi}(\mathbf{r}, \mathbf{r}_A, \omega)}{\partial z} \Phi^+(\mathbf{r}, \omega) \right]_{z_0} \mathrm{d}x\, \mathrm{d}y. \tag{21a}$$

With similar arguments, for S-wave sources in the upper half-space, (20b) may be approximated by

$$\Psi_h(\mathbf{r}_A, \omega) \approx 2 \iint_{-\infty}^{+\infty} \frac{1}{\rho\omega^2} \left[\frac{\partial \boldsymbol{\Gamma}^-_{\psi,\psi_h}(\mathbf{r}, \mathbf{r}_A, \omega)}{\partial z} \cdot \boldsymbol{\Psi}^+(\mathbf{r}, \omega) \right]_{z_0} \mathrm{d}x\, \mathrm{d}y. \tag{21b}$$

It should be emphasized that the extremely simple elastic expressions (21a) and (21b) hold for arbitrarily inhomogeneous anisotropic solids. The errors are of the same order as the negligence of multiply converted waves.

The Elastic Kirchhoff–Helmholtz Integral with Back-Propagating Green's Functions

The one-way elastic Rayleigh integrals discussed so far describe forward wavefield extrapolation: assuming the sources are in the upper half space $z < z_0$, the downgoing part of the elastic wavefield at z_0 is extrapolated away from the sources towards a point $\mathbf{r}_A$ in the lower half space $z > z_0$. In the following we derive expressions for elastic inverse wavefield extrapolation, towards the sources. For this derivation we follow the same path as in paper II. Therefore we introduce the back-propagating Green's functions $\mathbf{G}^*_m(\mathbf{r}, \mathbf{r}_A, \omega)$ and $\underset{\sim}{\boldsymbol{\theta}}^*_m(\mathbf{r}, \mathbf{r}_A, \omega)$, where * denotes complex conjugation.

We define a new vector function $\mathbf{Q}_m$, according to

$$\mathbf{Q}_m = \underset{\sim}{\tau}\mathbf{G}^*_m - \underset{\sim}{\boldsymbol{\theta}}^*_m \mathbf{U}, \tag{22}$$

where the components of $\mathbf{U}$, $\underset{\sim}{\tau}$, $\mathbf{G}_m$ and $\underset{\sim}{\boldsymbol{\theta}}_m$ satisfy equations (1) and (2) in V. Applying the theorem of Gauss (3a) to this vector function yields

$$U_m(\mathbf{r}_A, \omega) = \oint_S [\underset{\sim}{\tau}(\mathbf{r}, \omega)\mathbf{G}^*_m(\mathbf{r}, \mathbf{r}_A, \omega) - \underset{\sim}{\boldsymbol{\theta}}^*_m(\mathbf{r}, \mathbf{r}_A, \omega)\mathbf{U}(\mathbf{r}, \omega)]\mathbf{n}\, \mathrm{d}S. \tag{23}$$

This elastic Kirchhoff–Helmholtz integral is exact and is equivalent to elastic Kirchhoff–Helmholtz integral (4). However, as is shown later on in this paper, the back-propagating Green's functions in (23) appear to be a convenient choice when deriving inverse wavefield extrapolation operators.

In analogy with (12a) and (14a), we may derive the following two versions of the Kirchhoff–Helmholtz integrals:

$$\Phi(\mathbf{r}_A, \omega) = \oint_S [\underset{\sim}{\tau}(\mathbf{r}, \omega)\mathbf{G}^*_\varphi(\mathbf{r}, \mathbf{r}_A, \omega) - \underset{\sim}{\theta}^*_\varphi(\mathbf{r}, \mathbf{r}_A, \omega)\mathbf{U}(\mathbf{r}, \omega)] \cdot \mathbf{n}\, \mathrm{d}S \tag{24a}$$

and

$$\Psi_h(\mathbf{r}_A, \omega) = \oint_S [\underset{\sim}{\tau}(\mathbf{r}, \omega)\mathbf{G}^*_{\psi_h}(\mathbf{r}, \mathbf{r}_A, \omega) - \underset{\sim}{\theta}^*_{\psi_h}(\mathbf{r}, \mathbf{r}_A, \omega)\mathbf{U}(\mathbf{r}, \omega)] \cdot \mathbf{n}\, \mathrm{d}S, \tag{24b}$$

respectively. Kirchhoff–Helmholtz integrals (23), (24a) and (24b) can be summarized as

$$\Omega(\mathbf{r}_A, \omega) = \oint_S [\underset{\sim}{\tau}\mathbf{G}^*_\Omega - \underset{\sim}{\theta}^*_\Omega \mathbf{U}] \cdot \mathbf{n}\, \mathrm{d}S, \tag{25}$$

where $\Omega(\mathbf{r}_A, \omega)$ stands for $U_m(\mathbf{r}_A, \omega)$ or $\Phi(\mathbf{r}_A, \omega)$ or $\Psi_h(\mathbf{r}_A, \omega)$ and where $\mathbf{G}^*_\Omega$, $\underset{\sim}{\theta}^*_\Omega$ stand for $\mathbf{G}^*_m$, $\underset{\sim}{\theta}^*_m$ or $\mathbf{G}^*_\varphi$, $\underset{\sim}{\theta}^*_\varphi$ or $\mathbf{G}^*_{\psi_h}$, $\underset{\sim}{\theta}^*_{\psi_h}$, respectively.

One-Way Elastic Rayleigh Integrals for Inverse Wavefield Extrapolation

Elastic Kirchhoff–Helmholtz integral (25) is not yet applicable to the seismic situation because the 'seismic measurements' $\mathbf{U}(\mathbf{r}, \omega)$ and $\underset{\sim}{\tau}(\mathbf{r}, \omega)$ are never available at a closed surface. Consider the geometry of Fig. 6. Closed surface S consists of 'acquisition surface' S_0 of infinite extent, at $z = z_0$, a 'reference surface' S_1, also of infinite extent, at $z = z_1$, and a cylindrical surface S_2 with a vertical axis through A and radius R. Furthermore, we assume that the (secondary) sources are situated in the lower half-space below S_1. The contribution of the elastic Kirchhoff–Helmholtz integral over cylindrical surface S_2 to the wavefield in A vanishes if R goes to infinity. So for the geometry of Fig. 6 elastic Kirchhoff–Helmholtz integral (25) may be replaced by

$$\Omega(\mathbf{r}_A, \omega) = \Omega_0(\mathbf{r}_A, \omega) + \Delta\Omega(\mathbf{r}_A, \omega), \tag{26a}$$

where

$$\Omega_0(\mathbf{r}_A, \omega) = \iint_{-\infty}^{+\infty} [\boldsymbol{\theta}^*_{z,\Omega} \cdot \mathbf{U} - \mathbf{G}^*_\Omega \cdot \boldsymbol{\tau}_z]_{z_0}\, \mathrm{d}x\, \mathrm{d}y \tag{26b}$$

and

$$\Delta\Omega(\mathbf{r}_A, \omega) = -\iint_{-\infty}^{+\infty} [\boldsymbol{\theta}^*_{z,\Omega} \cdot \mathbf{U} - \mathbf{G}^*_\Omega \cdot \boldsymbol{\tau}_z]_{z_1}\, \mathrm{d}x\, \mathrm{d}y. \tag{26c}$$

Still this formulation is not suited for the seismic situation because $\mathbf{U}$ and $\boldsymbol{\tau}_z$ are not known at $z = z_1$. When $\Delta\Omega(\mathbf{r}_A, \omega)$, as defined in (26c), may be neglected, then (26b) describes inverse wavefield extrapolation (towards the secondary sources) from

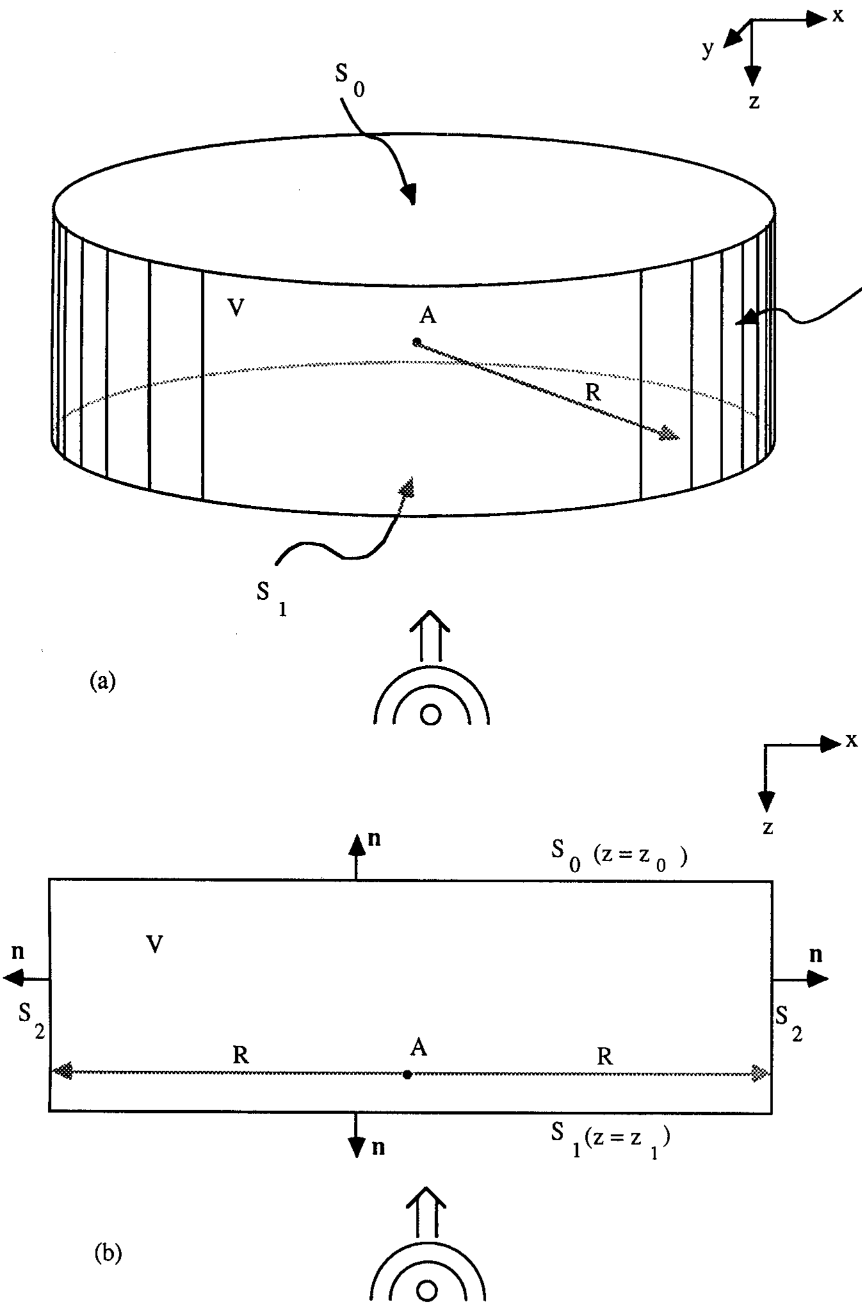

FIG. 6. Elastic inverse wavefield extrapolation (towards the sources below S_1) from acquisition surface S_0 to subsurface point A is described by elastic Kirchhoff–Helmholtz integral (26). Under certain conditions (discussed in the text) the contribution of this integral over S_1 can be neglected. (a) Perspective view. (b) Cross-section for $y = 0$.

acquisition surface S_0 to subsurface point A. In the following we analyse the expressions for $\Omega_0(\mathbf{r}_A, \omega)$ and $\Delta\Omega(\mathbf{r}_A, \omega)$ and show that, under certain conditions, the latter may be neglected. We assume that the medium is homogeneous, isotropic in (infinitely) thin regions around z_0 and around z_1. So in these regions the wavefields can be separated into downgoing and upgoing waves, which satisfy one-way wave equations (see also Appendix A). In addition, for the Green's functions we choose homogeneous and isotropic half spaces $z \leq z_0$ and $z \geq z_1$, which is allowed outside V. With this choice, the Green's functions at z_0 represent purely upgoing waves whilst the Green's functions at z_1 represent purely downgoing waves, which also satisfy one-way wave equations. Now, as (19b) was derived from (16), we can derive the following expressions from (26b) and (26c), respectively:

$$\Omega_0(\mathbf{r}_A, \omega) \approx 2 \iint_{-\infty}^{+\infty} \frac{1}{\rho\omega^2} \left[\left(\frac{\partial \Gamma_{\varphi,\Omega}^-}{\partial z} \right)^* \Phi^- + \left(\frac{\partial \mathbf{\Gamma}_{\psi,\Omega}^-}{\partial z} \right)^* \cdot \mathbf{\Psi}^- \right]_{z_0} \mathrm{d}x \, \mathrm{d}y \tag{27a}$$

and

$$\Delta\Omega(\mathbf{r}_A, \omega) \approx -2 \iint_{-\infty}^{+\infty} \frac{1}{\rho\omega^2} \left[\left(\frac{\partial \Gamma_{\varphi,\Omega}^+}{\partial z} \right)^* \Phi^+ + \left(\frac{\partial \mathbf{\Gamma}_{\psi,\Omega}^+}{\partial z} \right)^* \cdot \mathbf{\Psi}^+ \right]_{z_1} \mathrm{d}x \, \mathrm{d}y. \tag{27b}$$

Unlike (19b), equations (27a) and (27b) are not exact since in the derivation we assumed that the wavenumbers $k_{z,p}$ and $k_{z,s}$ (see Appendix A) satisfy

$$k_{z,p} = k_{z,p}^* \text{ and } k_{z,s} = k_{z,s}^* \text{ at } z_0 \text{ and at } z_1, \tag{27c}$$

which is only true for propagating waves. Hence, (27a) and (27b) represent spatially band-limited approximations of (26b) and (26c), respectively (evanescent waves are neglected). Let us for the moment assume that the elastic medium is homogeneous and isotropic everywhere in space. Because the sources are below z_1, the wavefield at z_1 is purely upgoing; hence, $\Phi^+ = 0$ and $\mathbf{\Psi}^+ = \mathbf{0}$ at z_1, and, consequently, $\Delta\Omega(\mathbf{r}_A, \omega) \approx 0$. Hence, according to (26a), for a homogeneous isotropic solid, inverse wavefield extrapolation from acquisition surface S_0 ($z = z_0$) to subsurface point A is described by the elastic Kirchhoff–Helmholtz integral (26b), or, equivalently, by the one-way elastic Rayleigh II integral (27a). In both expressions the only approximation is the spatial band-limitation (the negligence of evanescent waves). This imposes a restriction to the maximum obtainable spatial resolution (Berkhout 1984). When the elastic medium is arbitrarily inhomogeneous and anisotropic, then Φ^+ and $\mathbf{\Psi}^+$ at z_1 are generally non-zero, so $\Delta\Omega(\mathbf{r}_A, \omega)$, given by (27b), will generally not vanish.

Similar arguments as given in paper II lead to the conclusion that we may write for the upgoing wavefield at $\mathbf{r}_A$:

$$\Omega^-(\mathbf{r}_A, \omega) = \Omega_0(\mathbf{r}_A, \omega) + \Delta\Omega^-(\mathbf{r}_A, \omega), \tag{27d}$$

where the magnitude of $\Delta\Omega^-(\mathbf{r}_A, \omega)$ is proportional to multiply reflected waves. Hence, by neglecting $\Delta\Omega^-(\mathbf{r}_A, \omega)$, we obtain for the upgoing wavefield at $\mathbf{r}_A$

$$\Omega^-(\mathbf{r}_A, \omega) \approx 2 \iint_{-\infty}^{+\infty} \frac{1}{\rho\omega^2} \left[\left(\frac{\partial \Gamma_{\varphi,\Omega}^-}{\partial z} \right)^* \Phi^- + \left(\frac{\partial \mathbf{\Gamma}_{\psi,\Omega}^-}{\partial z} \right)^* \cdot \mathbf{\Psi}^- \right]_{z_0} \mathrm{d}x \, \mathrm{d}y. \tag{28}$$

Depending on the choice of the source for the Green's functions, Ω^- can represent either U_m^- for $m = 1, 2, 3$, or Φ^- or Ψ_h^-. We consider the latter two cases. If the Green's functions have a P-wave source at $\mathbf{r}_A$, then Ω^- represents the upgoing P-wave potential $\Phi^-(\mathbf{r}_A, \omega)$. If, in addition, the wavefield is generated by P-wave sources below z_1 then, analogous to (21a), equation (28) may be approximated by

$$\Phi^-(\mathbf{r}_A, \omega) \approx 2 \iint_{-\infty}^{+\infty} \frac{1}{\rho\omega^2} \left[\left(\frac{\partial \Gamma^-_{\varphi,\varphi}(\mathbf{r}, \mathbf{r}_A, \omega)}{\partial z} \right)^* \Phi^-(\mathbf{r}, \omega) \right]_{z0} \mathrm{d}x\, \mathrm{d}y. \tag{29a}$$

With similar arguments, for S-wave sources below z_1, (28) may be approximated by

$$\Psi_h^-(\mathbf{r}_A, \omega) \approx 2 \iint_{-\infty}^{+\infty} \frac{1}{\rho\omega^2} \left[\left(\frac{\partial \mathbf{\Gamma}^-_{\psi,\psi_h}(\mathbf{r}, \mathbf{r}_A, \omega)}{\partial z} \right)^* \cdot \mathbf{\Psi}^-(\mathbf{r}, \omega) \right]_{z0} \mathrm{d}x\, \mathrm{d}y. \tag{29b}$$

Summarizing, one-way elastic Rayleigh II integrals (29a) and (29b) describe inverse wavefield extrapolation (towards the source) from acquisition surface S_0 ($z = z_0$) to subsurface point A. Evanescent waves are neglected. In the case of an inhomogeneous, anisotropic medium, amplitude errors are introduced into the reconstructed upgoing wavefield at A. These errors are of the same order as the negligence of multiply reflected and multiply converted waves. First order amplitude effects, related to geometrical spreading and transmission/conversion at interfaces are all incorporated. In conclusion, assuming weak to moderate contrasts, integrals (29a) and (29b) describe non-recursive 'true amplitude' inverse extrapolation of primary P- and S-waves, respectively. In the situation of significant contrasts the 'error term' $\Delta\Omega^-(\mathbf{r}_A, \omega)$ should be estimated in an iterative way. Further discussion is beyond the scope of this paper. The reader is referred to Wapenaar and Berkhout (1989).

Examples of Elastic Inverse Wavefield Extrapolation

The practical implementation of elastic inverse wavefield extrapolation consists of the following steps (see also Fig. 1): (i) decomposition of the surface measurements; (ii) elimination of the surface multiples; (iii) computation of the inverse extrapolation operator (the Green's function); (iv) application of this operator to the decomposed surface measurements.

We discuss these steps with the aid of two numerical $2D$ examples. The first model consists of two half-spaces connected by a horizontal interface at $z = 600$ m shown in Fig. 7a. A P-wave (secondary) source is buried in the subsurface at a depth of $z = 1600$ m. The response of this source at surface level $z_0 = 0$ is shown in Figs 7b and 7c. They represent the vertical and horizontal component of the particle displacement, $u_z(x, z_0, t)$ and $u_x(x, z_0, t)$, respectively, both as a function of the lateral coordinate x and time t. The objective of the extrapolation process is to inverse extrapolate the recorded data from level z_0, through the subsurface, towards level z_A and thereby removing all propagating effects from this subsurface. It is general practice in seismic processing to use the vertical component of the displacement as a measure for the P-wave response, which is of course not correct. In addi-

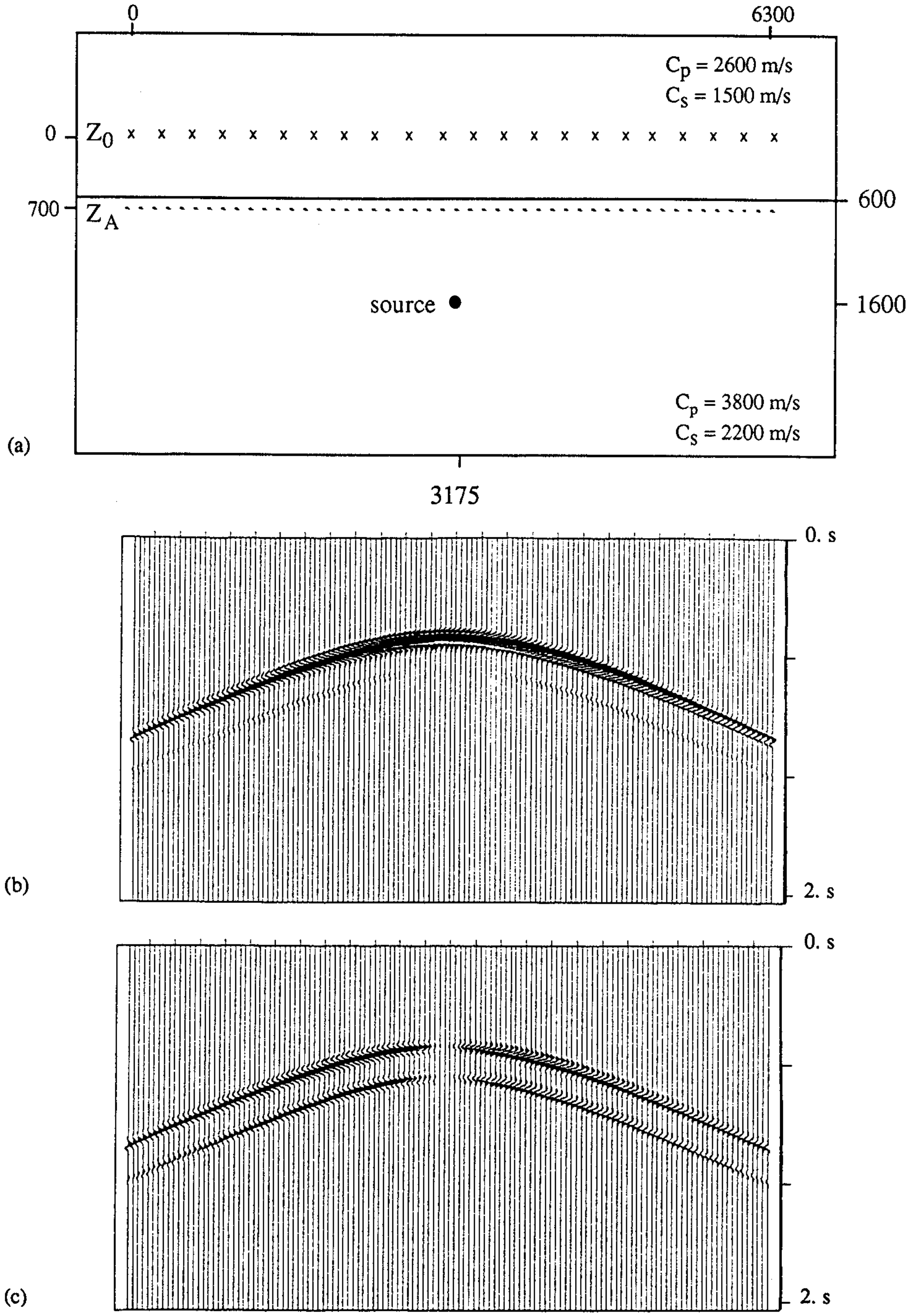

FIG. 7. (a) Two homogeneous half-spaces connected by a horizontal interface at $z = 600$ m. The black dot marks the position of a buried P-wave source at $z = 1600$ m. The crosses mark a receiver array at level z_0. (b) Recorded vertical displacement at level z_0 (pseudo P-data). (c) Recorded horizontal displacement at level z_0 (pseudo SV-data).

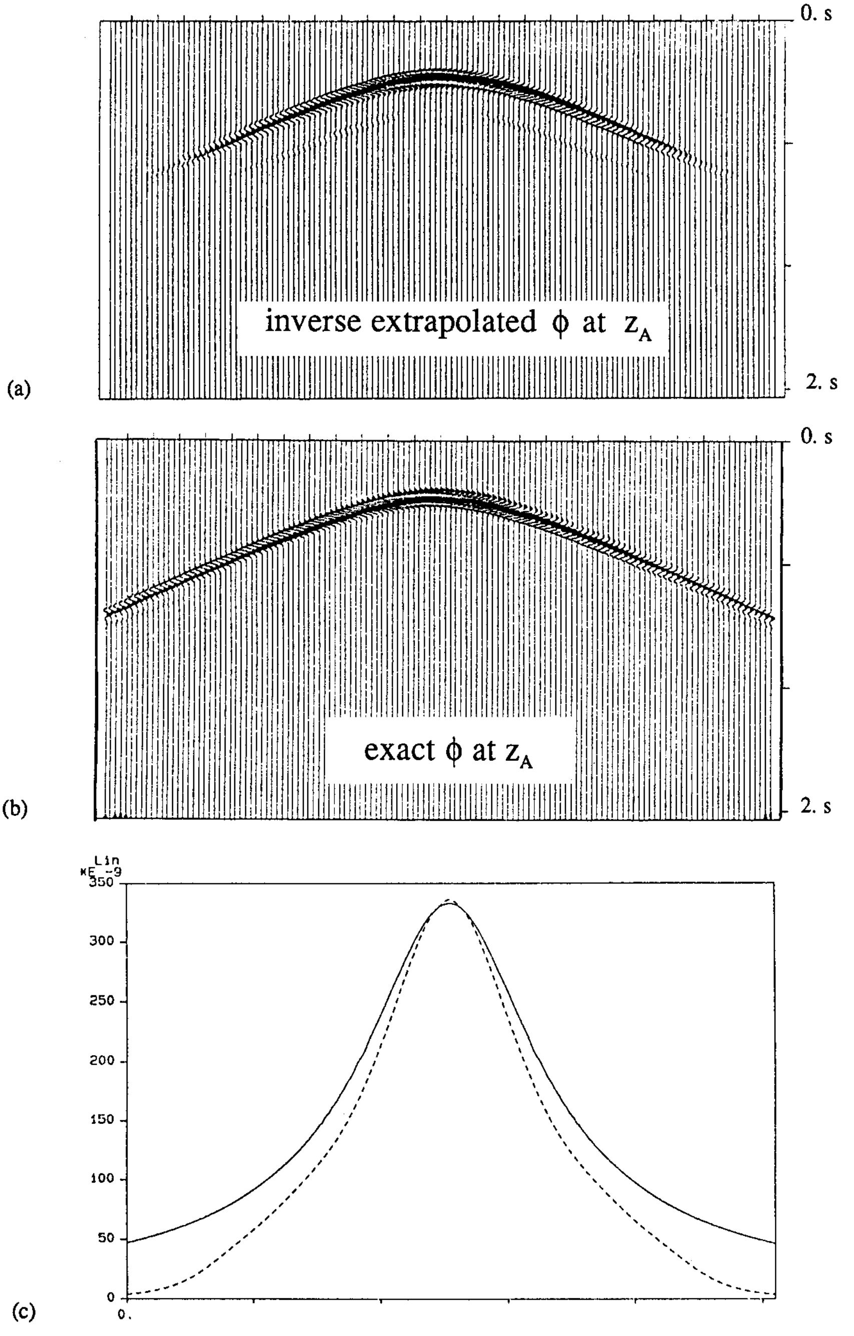

FIG. 8. (a) Acoustically inverse extrapolated pseudo P-data at z_A. (b) Exact upgoing P-wave at z_A. (c) Maximum amplitude per trace of Fig. 8a (dotted line) and exact result (solid line), Fig. 8b.

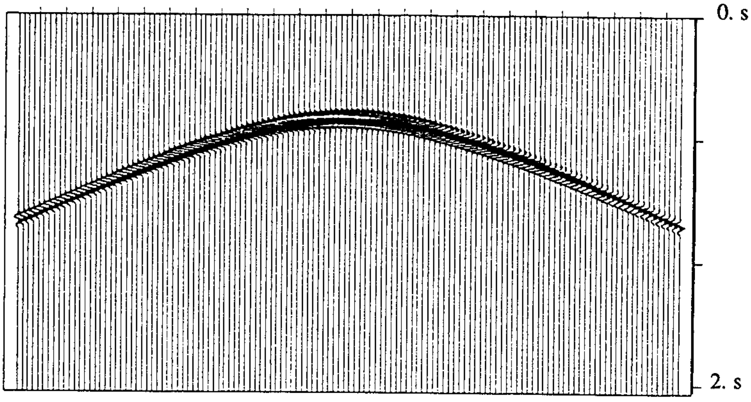

(a)

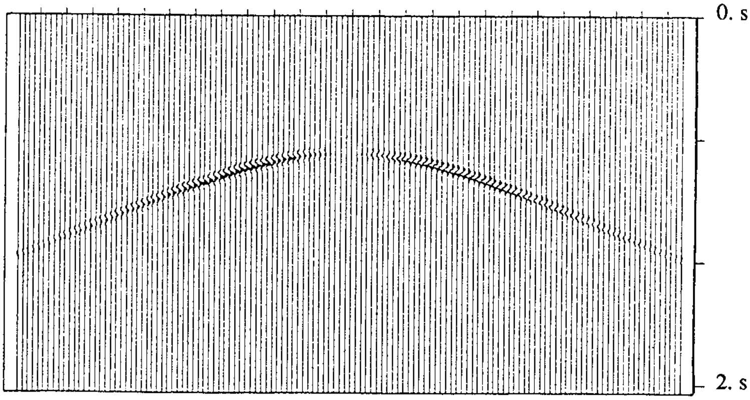

(b)

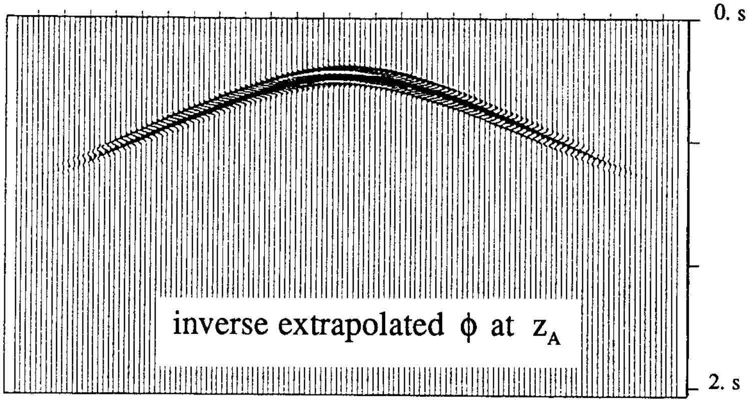

(c)

FIG. 9. (a) Decomposed upgoing ϕ-data at level z_0 (true P-data). (b) Decomposed upgoing ψ_y-data at level z_0 (true SV-data). (c) Elastically inverse extrapolated upgoing P-data at z_A. (d) Exact upgoing P-wave at z_A. (e) Maximum amplitude per trace of Fig. 9c (dotted line) and exact result (solid line), Fig. 9d.

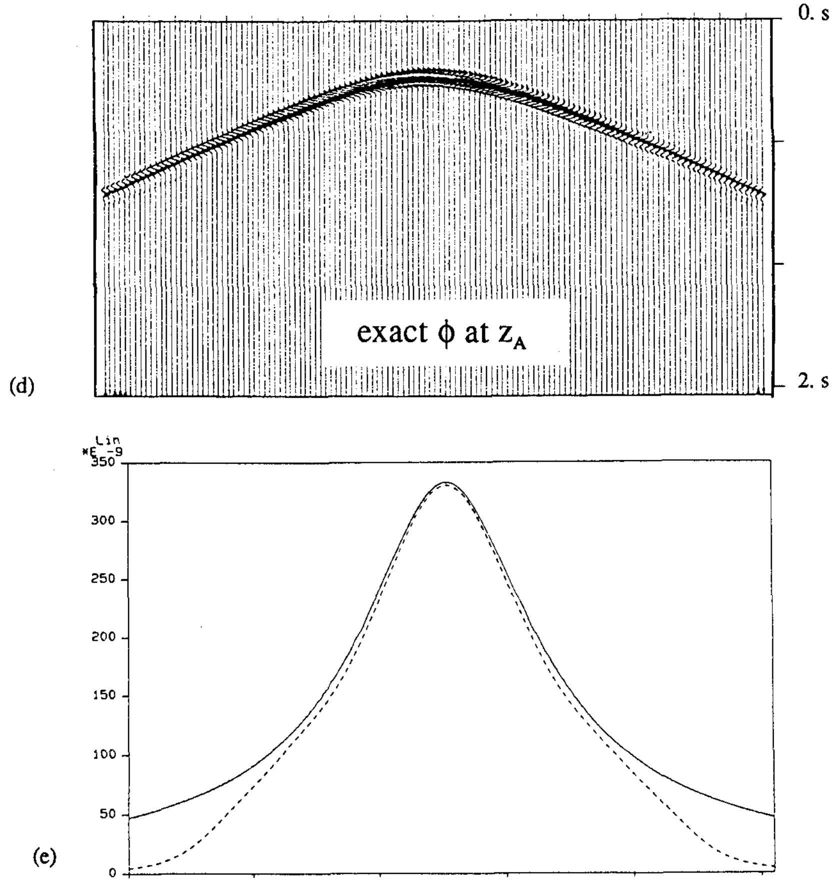

FIG. 9 (*continued*)

tion to that, acoustic Green's functions are used to extrapolate these pseudo P-data (u_z-data). Figure 8a shows the result of acoustic inverse extrapolation applied to the pseudo P-data of Fig. 7b. These inversely extrapolated data simulate the direct P-wave, measured at depth level z_A, above the P-wave source. For comparison in Fig. 8b the exact direct P-wave at level z_A is depicted. In Fig. 8c the amplitude cross-sections are compared. From these results we may conclude that the acoustic approach to inverse extrapolation of elastic data is not valid (artifacts in Fig. 8a; poor amplitude match in Fig. 8c).

Next we discuss the full elastic approach. First we decompose the surface measurements of Fig. 7 into one-way P-wave and S-wave potentials. The decomposed data at $z = z_0$ are shown in Figs 9a and 9b. They represent the upgoing potentials for P- and SV-waves, $\varphi^-(x, z_0, t)$ and $\psi_y^-(x, z_0, t)$, respectively (for the 2D-situation we denote S_y-waves as SV-waves). Because surface z_0 is reflection free we can omit the multiple elimination step. A discussion of the decomposition and elastic multiple elimination is beyond the scope of this paper. The reader is referred to Wapenaar *et* (1990).

To compute the elastic Green's functions we can in principle use any accurate forward modelling algorithm. In paper II we used the Gaussian beam method; here we use an elastic finite difference scheme (Kelly *et al.* 1976) to model the elastic Green's functions. In the frequency domain, we apply (29a), i.e. we apply the modelled elastic Green's functions to the true P-wave response (Fig. 9a). It can be seen from the inverse extrapolated result in Fig. 9c that the artefact is no longer present. In Fig. 9e the amplitude cross-section of Fig. 9c is compared with the amplitude cross section of the exact result (Fig. 9d). Note the significant improvement, compared with Fig. 8c. Also note that the amplitudes only match in the middle part. This is not a limitation of the inverse operator but of the finite aperture.

We did a second experiment on this model. Now, instead of using a buried *P*-source we use a buried SV-source. The response of this source at surface $z = z_0$ is shown in Figs 10a and 10b. Again in accordance with seismic practice, we first

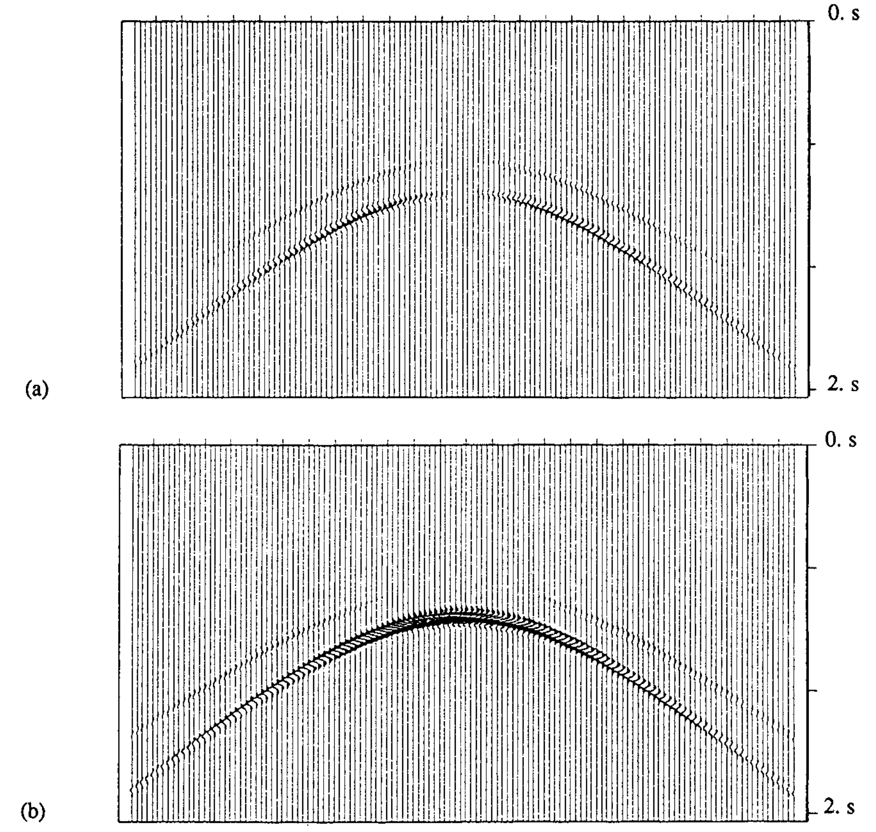

FIG. 10. Data related to a buried SV-source in Fig. 7a. (a) Recorded vertical displacement at level z_0 (pseudo P-data). (b) Recorded horizontal displacement at level z_0 (pseudo SV-data).

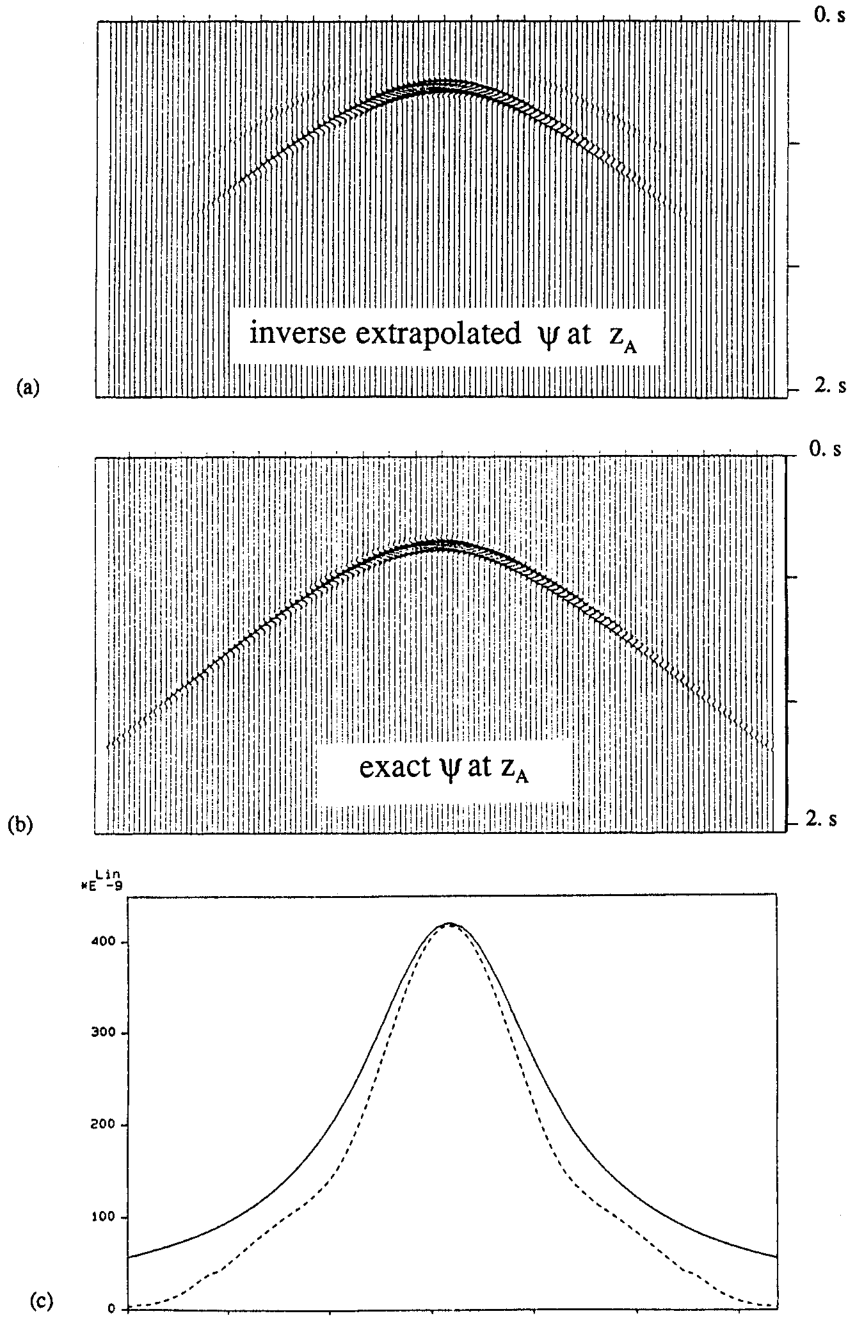

FIG. 11. (a) Acoustically inverse extrapolated pseudo SV-data at z_A. (b) Exact upgoing SV-wave at z_A. (c) Maximum amplitude per trace of Fig. 11a (dotted line) and exact result (solid line), Fig. 11b.

applied 'acoustic' inverse extrapolation (based on the S-wave velocity) to the pseudo SV-data (u_x-data). It can be seen from Fig. 11a that, just as in the first example, there is an artefact present in the inverse extrapolated data, but now this concerns the first event in the data which corresponds to the converted *P*-data in Fig. 10b. Applying (29b) to the decomposed upgoing SV-wave potential (Fig. 12b) results in the data set depicted in Fig. 12c. It can be seen that now the artefact has disappeared. We see from Fig. 12e that there is still an amplitude mismatch within the aperture. Apparently the assumption of 'moderate contrasts' is violated.

In the last experiment we use a more complex model. The model is displayed in Fig. 13a. A plane P-wave source is buried at the depth of $z = 2000$ m. The response at z_0 is shown in Figs 13b and 13c. Using equation (29a) with elastic Green's functions and the decomposed *P*-data (Fig. 14a) results in the data set depicted in

(a)

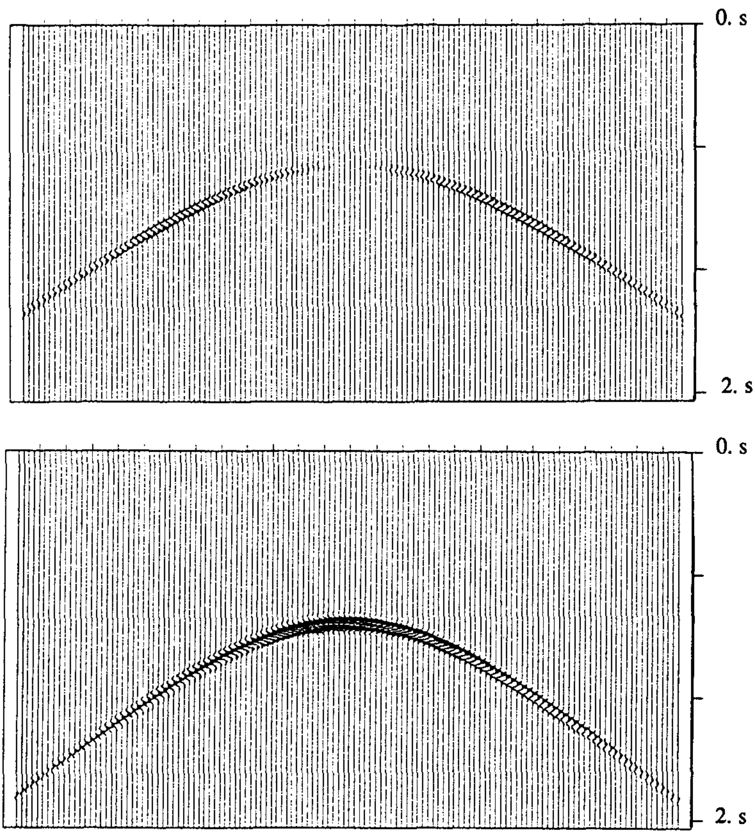

(b)

FIG. 12. (a) Decomposed upgoing ϕ-data at level z_0 (true P-data). (b) Decomposed upgoing ψ_y-data at level z_0 (true SV-data). (c) Elastically inverse extrapolated upgoing SV-data at z_A. (d) Exact upgoing SV-wave at z_A. (e) Maximum amplitude per trace of Fig. 12c (dotted line) and exact result (solid line), Fig. 12d.

(c)

(d)

(e)

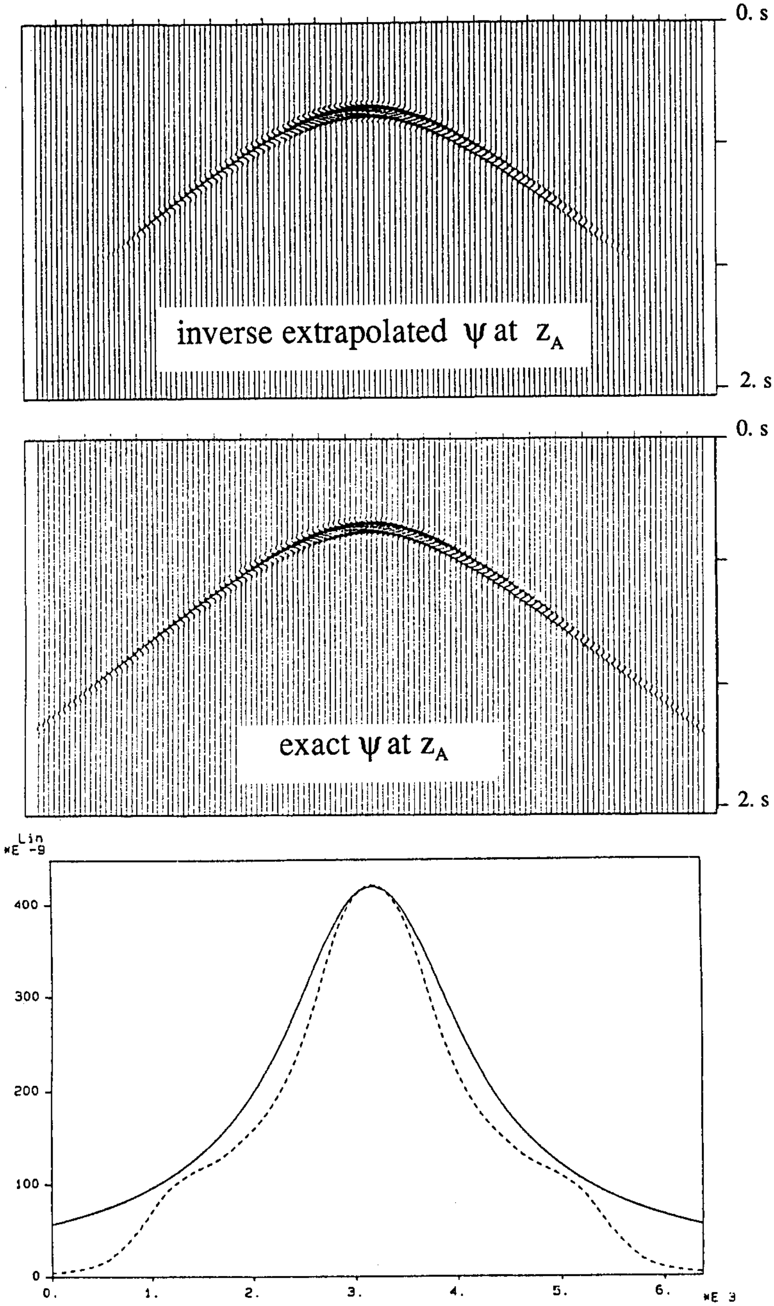

FIG. 12 (*continued*)

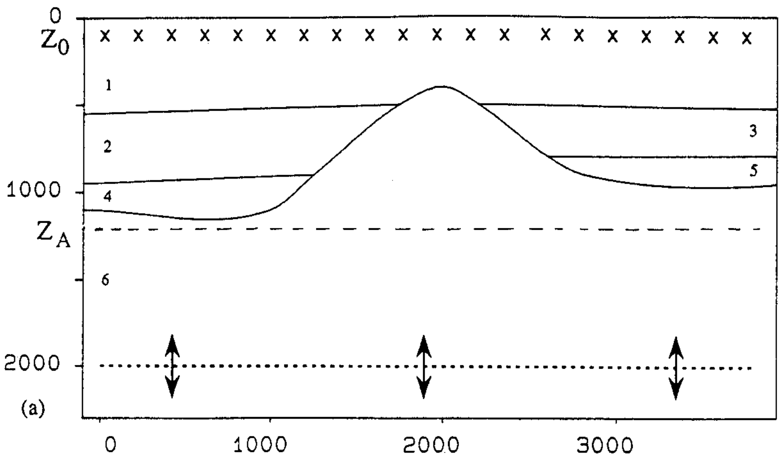

layer nr	velocities
1	Cp = 2600 m/s Cs = 1500 m/s
2	Cp = 3200 m/s Cs = 1900 m/s
3	Cp = 3200 m/s Cs = 1900 m/s
4	Cp = 2800 m/s Cs = 1600 m/s
5	Cp = 3000 m/s Cs = 1800 m/s
6	Cp = 3600 m/s Cs = 2078 m/s

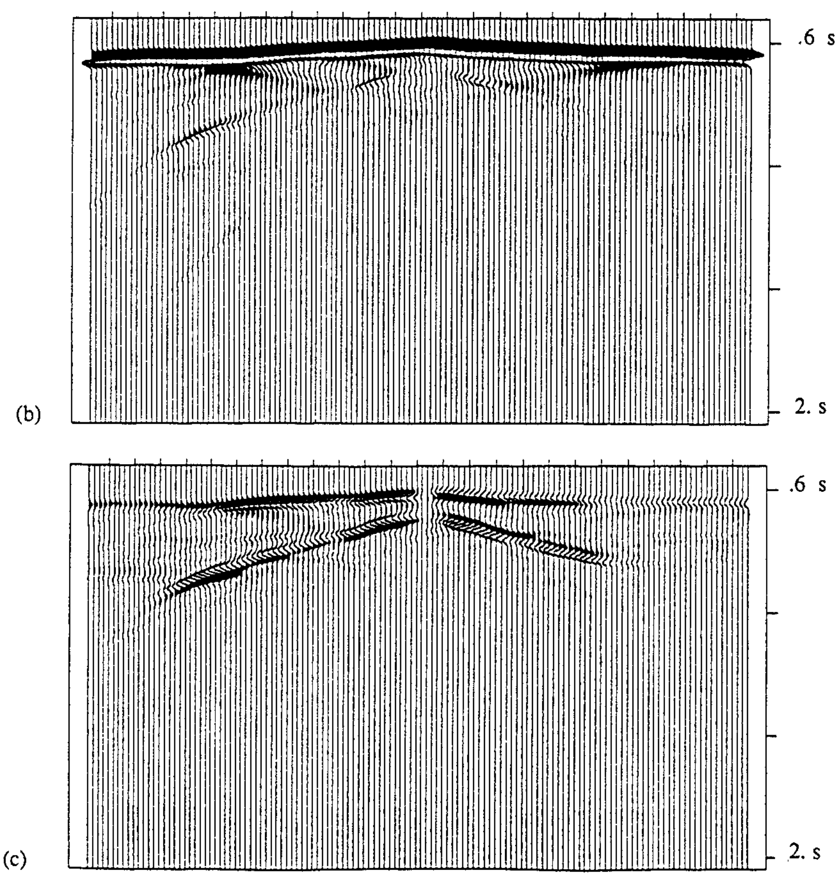

FIG. 13. (a) Complex overburden. A plane P-wave source is buried at $z = 2000$ m. (b) Recorded vertical displacement at level z_0 (pseudo P-data). (c) Recorded horizontal displacement at level z_0 (pseudo SV-data).

Fig. 14c. Note that the distorting propagation effects of the elastic overburden have been properly removed (compare with Fig. 13b). The amplitude match with the exact result is very good (Fig. 14e).

Finally, using the same model we now consider a buried plane SV-wave source at $z = 2000$ m. The response at level z_0 is shown in Figs 15b and 15c. Using (29b), extrapolation of the decomposed SV-data (Fig. 16b) results in the data set displayed in Fig. 16c. The distorting propagation effects of the elastic overburden have been removed for the greater part (compare with Fig. 15c). The amplitude match (Fig. 16e) is less accurate than in the P-wave example (Fig. 14e). Again, apparently the assumption of 'moderate contrasts' is violated.

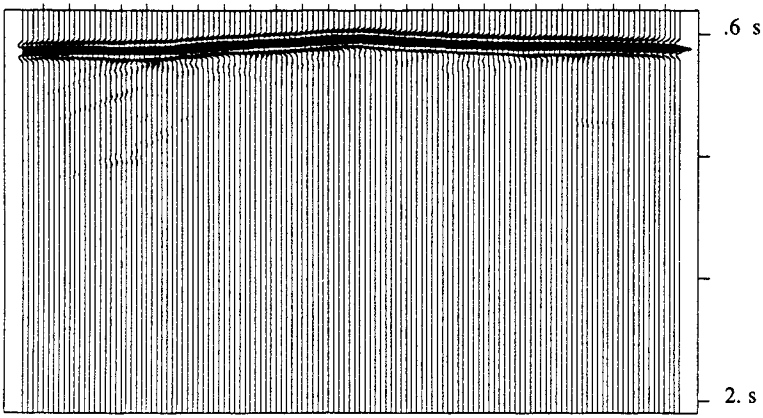

(a)

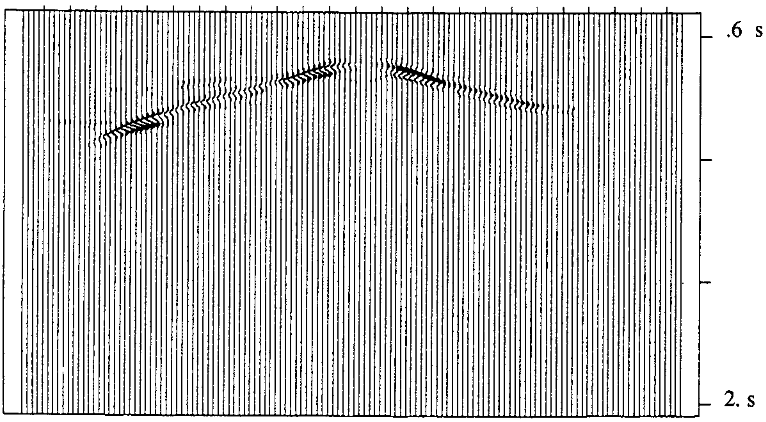

(b)

FIG. 14. (a) Decomposed upgoing ϕ-data at level z_0 (true P-data). (b) Decomposed upgoing ψ_y-data at level z_0 (true SV-data). (c) Elastically inverse extrapolated upgoing P-data at z_A. (d) Exact upgoing P-wave at z_A. (c) Maximum amplitude per trace of Fig. 14c (dotted line) and exact result (solid line), Fig. 14d.

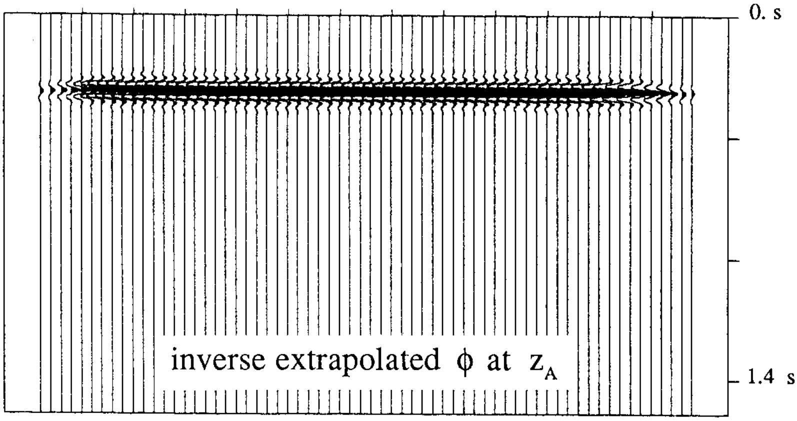

(c)

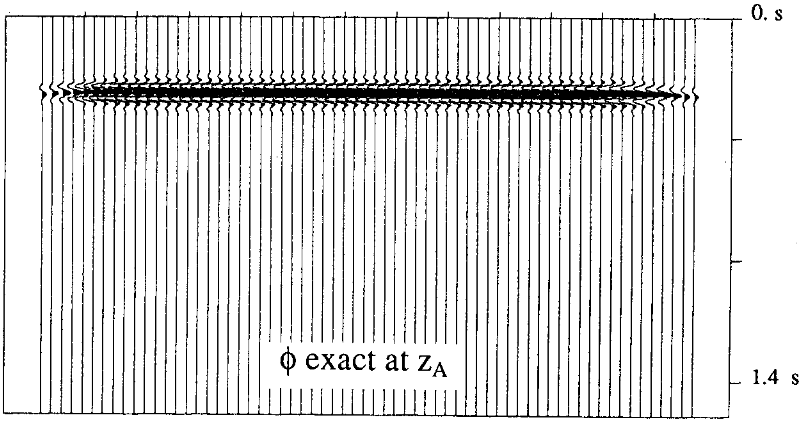

(d)

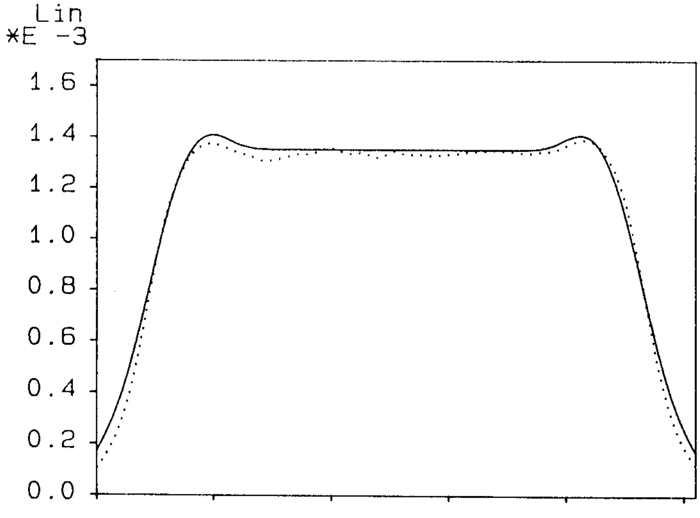

(e)

FIG. 14 *(continued)*

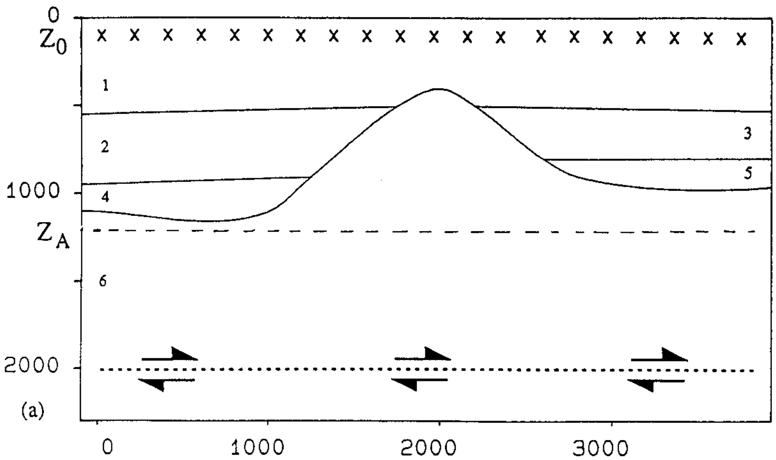

layer nr	velocities
1	Cp = 2600 m/s Cs = 1500 m/s
2	Cp = 3200 m/s Cs = 1900 m/s
3	Cp = 3200 m/s Cs = 1900 m/s
4	Cp = 2800 m/s Cs = 1600 m/s
5	Cp = 3000 m/s Cs = 1800 m/s
6	Cp = 3600 m/s Cs = 2078 m/s

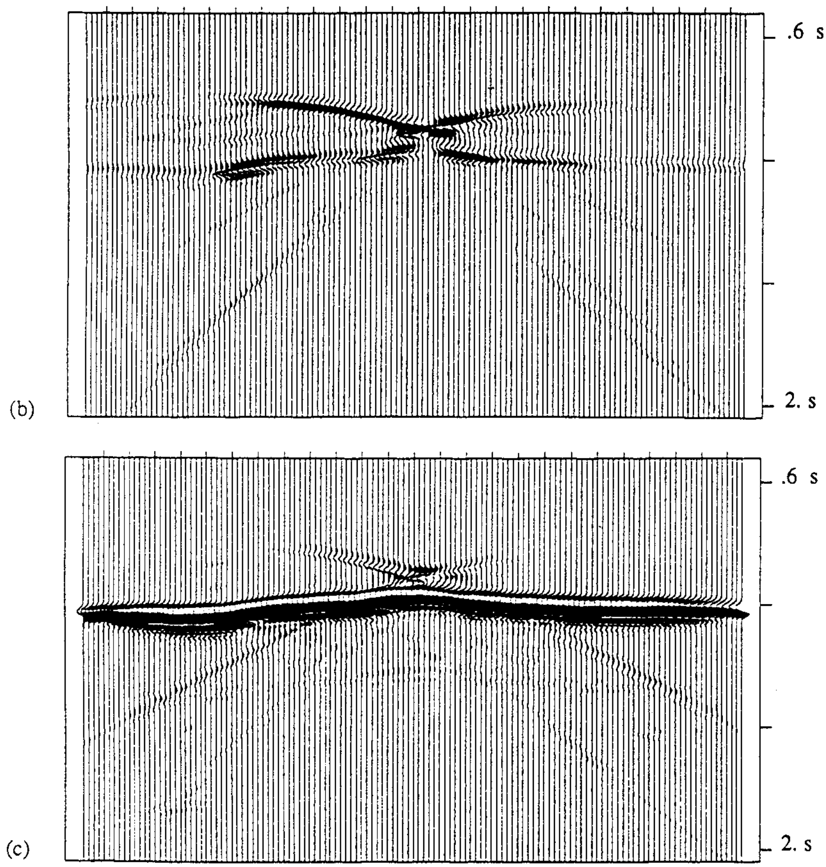

FIG. 15. (a) Complex overburden. A plane SV-wave source is buried at $z = 2000$ m. (b) Recorded vertical displacement at level z_0 (pseudo P-data). (c) Recorded horizontal displacement at level z_0 (pseudo SV-data).

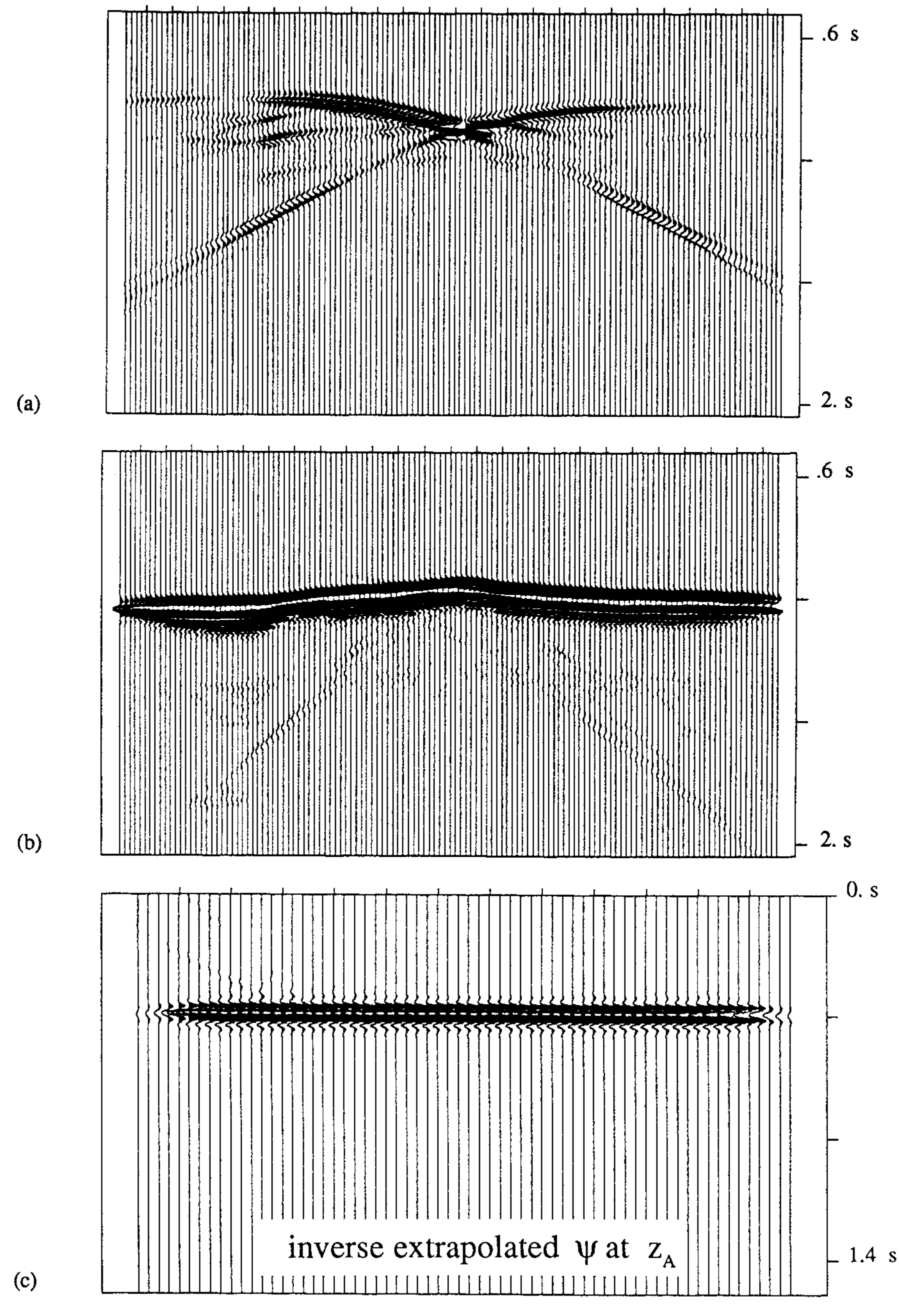

FIG. 16. (a) Decomposed upgoing ϕ-data at level z_0 (true P-data). (b) Decomposed upgoing ψ_y-data at level z_0 (true SV-data). (c) Elastically inverse extrapolated upgoing SV-data at z_A. (d) Exact upgoing SV-wave at z_A. (e) Maximum amplitude per trace of Fig. 16c (dotted line) and exact result (solid line), Fig. 16d.

(d)

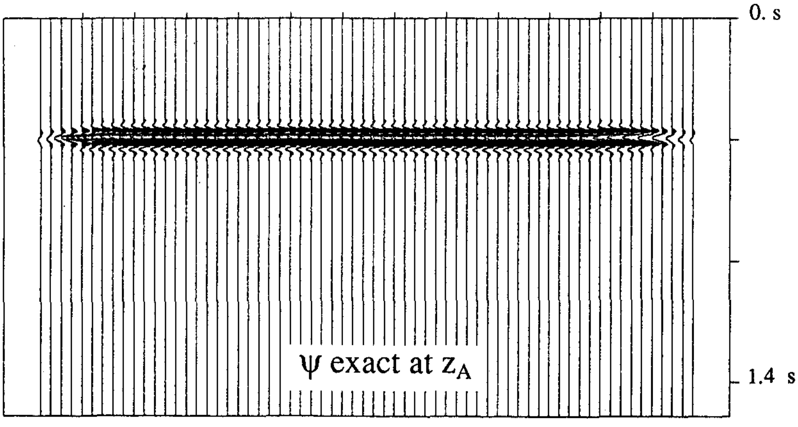

(e)

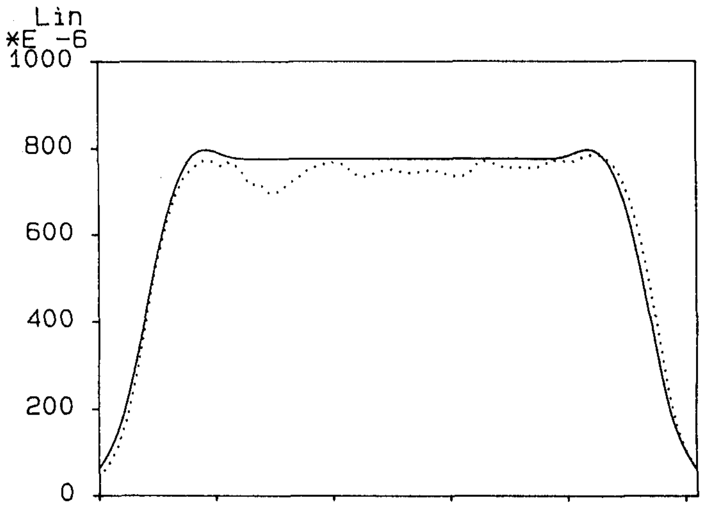

FIG. 16 *(continued)*

CONCLUSIONS

1. We have introduced Green's functions for P- and S-waves in 3D inhomogeneous anisotropic solid media. $\Gamma_{\varphi,\varphi}(\mathbf{r}, \mathbf{r}_A, \omega)$ represents the monochromatic P-wave response at 'observation point' $\mathbf{r}$ related to a P-wave source at Green's 'source point' $\mathbf{r}_A$ (see Fig. 3d). $\Gamma_{\psi,\psi_h}(\mathbf{r}, \mathbf{r}_A, \omega)$ represents the monochromatic S-wave response at 'observation point' $\mathbf{r}$, related to an S_h-wave source at Green's 'source point' $\mathbf{r}_A$ (an S_h-wave is polarized in the plane perpendicular to the h-axis, see Fig. 3h). These Green's functions satisfy the following reciprocity relations

$$\Gamma_{\varphi,\varphi}(\mathbf{r}_B, \mathbf{r}_A, \omega) = \Gamma_{\varphi,\varphi}(\mathbf{r}_A, \mathbf{r}_B, \omega) \tag{30a}$$

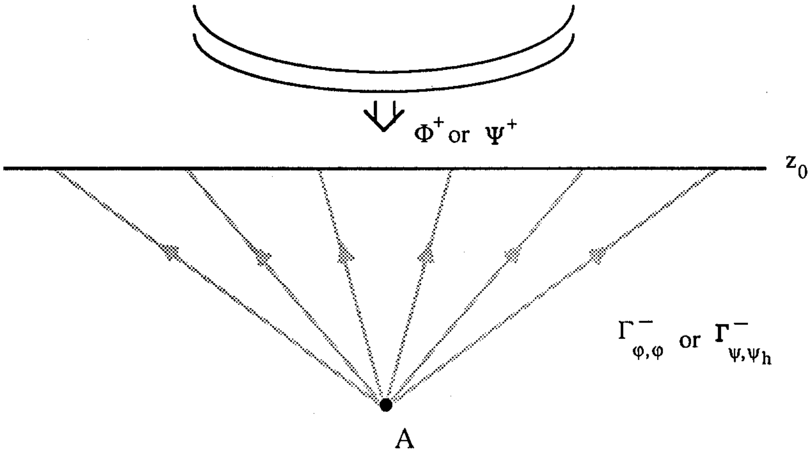

FIG. 17. Forward extrapolation of P- or S-waves from z_0 to A (equation 31).

and

$$\Gamma_{\psi_k,\psi_h}(\mathbf{r}_B, \mathbf{r}_A, \omega) = \Gamma_{\psi_h,\psi_k}(\mathbf{r}_A, \mathbf{r}_B, \omega), \tag{30b}$$

where Γ_{ψ_k,ψ_h} represents the k-component of $\boldsymbol{\Gamma}_{\psi,\psi_h}$.

2. We derived one-way elastic Rayleigh II integrals for forward extrapolation of P- and S-waves (Fig. 17)

$$\Phi(\mathbf{r}_A, \omega) \approx 2 \iint_{-\infty}^{+\infty} \frac{1}{\rho\omega^2} \left[\left(\frac{\partial \Gamma^-_{\varphi,\varphi}}{\partial z} \right) \Phi^+ \right]_{z_0} \mathrm{d}x \, \mathrm{d}y \tag{31a}$$

and

$$\Psi_h(\mathbf{r}_A, \omega) \approx 2 \iint_{-\infty}^{+\infty} \frac{1}{\rho\omega^2} \left[\left(\frac{\partial \boldsymbol{\Gamma}^-_{\psi,\psi_h}}{\partial z} \right) \cdot \boldsymbol{\Psi}^+ \right]_{z_0} \mathrm{d}x \, \mathrm{d}y. \tag{31b}$$

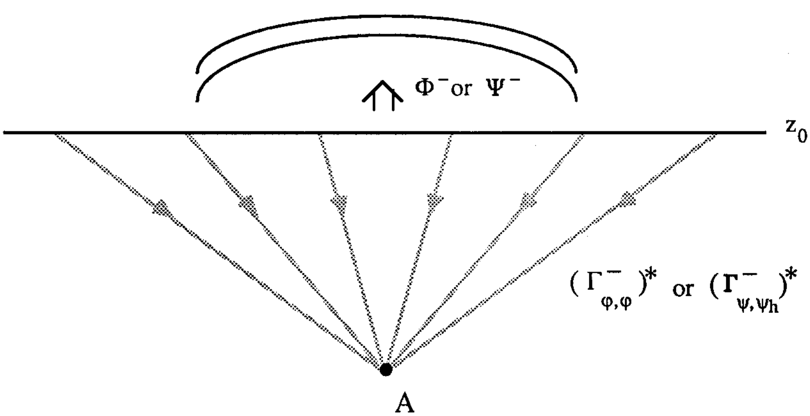

FIG. 18. Inverse extrapolation of P- or S-waves from z_0 to A (equation 32).

Assuming P-wave sources in the upper half-space $z < z_0$, equation (31a) expresses the (monochromatic) P-wave at $\mathbf{r}_A$ (in the lower half-space $z \geq z_0$) in terms of the downgoing P-wave at z_0 and the upgoing Green's P-wave at z_0. Assuming S-wave sources in the upper half space, (31b) expresses the (monochromatic) S_h-wave at $\mathbf{r}_A$ in terms of the downgoing S-wave at z_0 and the upgoing Green's S-wave at z_0.

3. We derived one-way elastic Rayleigh II integrals for inverse extrapolation of P- and S-waves (Fig. 18)

$$\Phi^-(\mathbf{r}_A, \omega) \approx 2 \iint_{-\infty}^{+\infty} \frac{1}{\rho\omega^2} \left[\left(\frac{\partial \Gamma^-_{\varphi,\varphi}}{\partial z} \right)^* \Phi^- \right]_{z0} \mathrm{d}x \, \mathrm{d}y \tag{32a}$$

and

$$\Psi_h^-(\mathbf{r}_A, \omega) \approx 2 \iint_{-\infty}^{+\infty} \frac{1}{\rho\omega^2} \left[\left(\frac{\partial \boldsymbol{\Gamma}^-_{\psi,\psi_h}}{\partial z} \right)^* \cdot \boldsymbol{\Psi}^- \right]_{z0} \mathrm{d}x \, \mathrm{d}y. \tag{32b}$$

Assuming P-wave sources below z_A, (32a) expresses the upgoing P-wave at $\mathbf{r}_A$ in terms of the upgoing P wave at z_0 and the back-propagating upgoing Green's P-wave at z_0. Assuming S-wave sources below z_A, (32b) expresses the upgoing S_h-wave at $\mathbf{r}_A$ in terms of the upgoing S-wave at z_0 and the back-propagating upgoing Green's S-wave at z_0.

The underlying assumption for (31) and (32) is that the contrasts in the inhomogeneous, anisotropic medium between z_0 and z_A are weak to moderate. For the examples that we showed, this assumption appears to be more severe for S-wave extrapolation than for P-wave extrapolation. In the situation of significant contrasts the results can be improved by estimating the 'error term' $\Delta\Omega^-(\mathbf{r}_A, \omega)$ in (27d) in an iterative way.

We expect that the forward and inverse one-way extrapolation operators for primary P- and S-waves will play a major role in the practice of prestack migration of decomposed elastic data (Berkhout and Wapenaar 1988, see also Fig. 1).

Acknowledgements

We would like to thank Professor A. J. Berkhout, director of the Laboratory of Seismics and Acoustics, for many stimulating discussions. This research was supported by the Royal Dutch Academy of Sciences (KNAW) and by the sponsors of the TRITON project.

Appendix A

One-way elastic wave equations for P- and S-waves

In a homogeneous, isotropic source-free region the full elastic wave equation reads (Pilant 1979)

$$K_c \nabla(\nabla \cdot \mathbf{U}) - \mu \nabla \times \nabla \times \mathbf{U} + \rho\omega^2 \mathbf{U} = \mathbf{0}, \tag{A1}$$

where $K_c = \lambda + 2\mu$. We define Lamé potentials Φ and $\boldsymbol{\Psi}$ for P- and S-waves, respectively, according to

$$\mathbf{U} \triangleq (\rho\omega^2)^{-1}[\nabla\Phi + \nabla \times \boldsymbol{\Psi}], \tag{A2a}$$

where

$$\nabla \cdot \boldsymbol{\Psi} \triangleq 0. \tag{A2b}$$

The factor $(\rho\omega^2)^{-1}$ is generally omitted. The reason that we use this factor is because in the limiting case of an ideal fluid ($\mu = 0$) the Lamé potential Φ, as defined in (A2a), represents the acoustic pressure. This can be clearly seen in (A5a) below. From (A2a) and (A2b) we obtain

$$\nabla \cdot \mathbf{U} = (\rho\omega^2)^{-1}\nabla^2\Phi \tag{A3a}$$

and

$$\nabla \times \mathbf{U} = (\rho\omega^2)^{-1}\nabla \times \nabla \times \boldsymbol{\Psi}, \tag{A3b}$$

or, with (A2b)

$$\nabla \times \mathbf{U} = -(\rho\omega^2)^{-1}\nabla^2\boldsymbol{\Psi}. \tag{A3c}$$

Substituting these expressions in (A1) yields two independent equations for P- and S-waves, respectively,

$$\nabla^2\Phi + \left(\frac{\rho\omega^2}{K_c}\right)\Phi = 0 \tag{A4a}$$

and

$$\nabla^2\boldsymbol{\Psi} + \left(\frac{\rho\omega^2}{\mu}\right)\boldsymbol{\Psi} = \mathbf{0} \tag{A4b}$$

or

$$\nabla^2\Psi_k + \left(\frac{\rho\omega^2}{\mu}\right)\Psi_k = 0. \tag{A4c}$$

From (A3) and (A4) we obtain

$$\Phi = -K_c \nabla \cdot \mathbf{U} \tag{A5a}$$

or

$$\Phi = -K_c\, \partial_i U_i$$

and

$$\boldsymbol{\Psi} = \mu\nabla \times \mathbf{U} \tag{A5b}$$

or

$$\Psi_k = -\mu\varepsilon_{kij}\, \partial_j U_i.$$

Throughout this paper, (A5a) and (A5b), respectively, are used as alternative definitions of P- and S-wave potentials.

In the wavenumber-frequency domain (k_x, k_y, z; ω), (A4a) and (A4b) may be written as

$$\frac{\partial^2 \tilde{\Phi}}{\partial z^2} = -k_{z,p}^2 \tilde{\Phi} \tag{A6a}$$

and

$$\frac{\partial^2 \tilde{\boldsymbol{\Psi}}}{\partial z^2} = -k_{z,s}^2 \tilde{\boldsymbol{\Psi}}, \tag{A6b}$$

respectively, where

$$k_{z,p}^2 = \frac{\rho\omega^2}{\mathbf{K}_c} - k_x^2 - k_y^2 \tag{A6c}$$

and

$$k_{z,s}^2 = \frac{\rho\omega^2}{\mu} - k_x^2 - k_y^2. \tag{A6d}$$

Now the one-way wave equations follow immediately:

$$\frac{\partial \tilde{\Phi}^\pm}{\partial z} = \mp j k_{z,p} \tilde{\Phi}^\pm \tag{A7a}$$

and

$$\frac{\partial \tilde{\boldsymbol{\Psi}}^\pm}{\partial z} = \mp j k_{z,s} \tilde{\boldsymbol{\Psi}}^\pm. \tag{A7b}$$

With definitions (A2*a*), (A2b) and one-way wave equations (A7a) and (A7b), we may write for the displacement in the wavenumber–frequency domain

$$\tilde{\mathbf{U}}^\pm = \tilde{\mathbf{D}}_p^\pm \tilde{\Phi}^\pm + \tilde{\underset{\sim}{\mathbf{D}}}_s^\pm \tilde{\boldsymbol{\Psi}}^\pm, \tag{A8a}$$

where

$$-jk_x \tilde{\Psi}_x^\pm - jk_y \tilde{\Psi}_y^\pm \mp jk_{z,s} \tilde{\Psi}_z^\pm = 0, \tag{A8b}$$

$$\tilde{\mathbf{D}}_p^\pm = \frac{1}{\rho\omega^2} \begin{bmatrix} -jk_x \\ -jk_y \\ \mp jk_{z,p} \end{bmatrix} \tag{A8c}$$

and

$$\tilde{\underset{\sim}{\mathbf{D}}}_s^\pm = \frac{1}{\rho\omega^2} \begin{bmatrix} 0 & \pm jk_{z,s} & -jk_y \\ \mp jk_{z,s} & 0 & jk_x \\ jk_y & -jk_x & 0 \end{bmatrix}. \tag{A8d}$$

Finally we give a similar expression for the traction in the wavenumber–frequency domain

$$\tilde{\boldsymbol{\tau}}_z^{\pm} = \tilde{\mathbf{E}}_p^{\pm}\tilde{\Phi}^{\pm} + \tilde{\underset{\sim}{\mathbf{E}}}_s^{\pm}\tilde{\boldsymbol{\Psi}}^{\pm}. \tag{A9a}$$

Here operators $\tilde{\mathbf{E}}_p^{\pm}$ and $\tilde{\underset{\sim}{\mathbf{E}}}_s^{\pm}$ are related to operators $\tilde{\mathbf{D}}_p^{\pm}$ and $\tilde{\underset{\sim}{\mathbf{D}}}_s^{\pm}$, respectively, via the stress-displacement relations in the wavenumber–frequency domain, according to

$$\tilde{\mathbf{E}}_p^{\pm} = \tilde{\underset{\sim}{\mathbf{K}}}_p^{\pm}\tilde{\mathbf{D}}_p^{\pm} \tag{A9b}$$

and

$$\tilde{\underset{\sim}{\mathbf{E}}}_s^{\pm} = \tilde{\underset{\sim}{\mathbf{K}}}_s^{\pm}\tilde{\underset{\sim}{\mathbf{D}}}_s^{\pm}, \tag{A9c}$$

where

$$\tilde{\underset{\sim}{\mathbf{K}}}_p^{\pm} = \begin{bmatrix} \mp\mu j k_{z,p} & 0 & -\mu j k_x \\ 0 & \mp\mu j k_{z,p} & -\mu j k_y \\ -\lambda j k_x & -\lambda j k_y & \mp(\lambda + 2\mu) j k_{z,p} \end{bmatrix} \tag{A9d}$$

and

$$\tilde{\underset{\sim}{\mathbf{K}}}_s^{\pm} = \begin{bmatrix} \mp\mu j k_{z,s} & 0 & -\mu j k_x \\ 0 & \mp\mu j k_{z,s} & -\mu j k_y \\ -\lambda j k_x & -\lambda j k_y & \mp(\lambda + 2\mu) j k_{z,s} \end{bmatrix}. \tag{A9e}$$

APPENDIX B

Substitution of the one-way elastic wave equations in the two-way elastic Kirchhoff–Helmholtz integral

Applying the 2D version of Parseval's theorem (Dudgeon and Mersereau 1984) to elastic Kirchhoff–Helmholtz integral (17) yields

$$\Omega(\mathbf{r}_A, \omega) = \left(\frac{1}{2\pi}\right)^2 \iint_{-\infty}^{+\infty} [\tilde{\boldsymbol{\theta}}'^{-}_{z,\Omega} \cdot (\tilde{\mathbf{U}}^{+} + \tilde{\mathbf{U}}^{-}) - \tilde{\mathbf{G}}'^{-}_{\Omega} \cdot (\tilde{\boldsymbol{\tau}}_z^{+} + \tilde{\boldsymbol{\tau}}_z^{-})]_{z_0}\, dk_x\, dk_y, \tag{B1a}$$

where the tilde ($\sim$) denotes the wavenumber–frequency domain:

$$\tilde{\mathbf{U}}^{\pm} = \tilde{\mathbf{U}}^{\pm}(k_x, k_y, z; \omega) \tag{B1b}$$

$$\tilde{\boldsymbol{\tau}}_z^{\pm} = \tilde{\boldsymbol{\tau}}_z^{\pm}(k_x, k_y, z; \omega) \tag{B1c}$$

and where the prime (′) denotes that k_x and k_y are replaced by $-k_x$ and $-k_y$, respectively:

$$\tilde{\mathbf{G}}'^{-}_{\Omega} = \tilde{\mathbf{G}}^{-}_{\Omega}(-k_x, -k_y, z; x_A, y_A, z_A; \omega) \tag{B1d}$$

$$\tilde{\boldsymbol{\theta}}'^{-}_{z,\Omega} = \tilde{\boldsymbol{\theta}}^{-}_{z,\Omega}(-k_x, -k_y, z; x_A, y_A, z_A; \omega) \tag{B1e}$$

We can now elegantly make use of the one-way wave equations for P- and S-waves (see also Appendix A)

$$\tilde{\mathbf{U}}^{\pm} = \tilde{\mathbf{D}}_p^{\pm}\tilde{\Phi}^{\pm} + \tilde{\underset{\sim}{\mathbf{D}}}_s^{\pm}\tilde{\mathbf{\Psi}}^{\pm}, \tag{B2a}$$

$$\tilde{\boldsymbol{\tau}}_z^{\pm} = \tilde{\mathbf{E}}_p^{\pm}\tilde{\Phi}^{\pm} + \tilde{\underset{\sim}{\mathbf{E}}}_s^{\pm}\tilde{\mathbf{\Psi}}^{\pm}, \tag{B2b}$$

$$\tilde{\mathbf{G}}_{\Omega}^{\prime -} = -\tilde{\mathbf{D}}_p^{+}\tilde{\Gamma}_{\varphi,\Omega}^{\prime -} - \tilde{\underset{\sim}{\mathbf{D}}}_s^{+}\tilde{\mathbf{\Gamma}}_{\psi,\Omega}^{\prime -} \tag{B2c}$$

and

$$\tilde{\boldsymbol{\theta}}_{z,\Omega}^{\prime -} = \tilde{\mathbf{E}}_p^{+}\tilde{\Gamma}_{\varphi,\Omega}^{\prime -} + \tilde{\underset{\sim}{\mathbf{E}}}_s^{+}\tilde{\mathbf{\Gamma}}_{\psi,\Omega}^{\prime -} \tag{B2d}$$

at $z = z_0$. With the definitions in Appendix A it can be verified that

$$[\tilde{\boldsymbol{\theta}}_{z,\Omega}^{\prime -}\cdot\tilde{\mathbf{U}}^{-} - \tilde{\mathbf{G}}_{\Omega}^{\prime -}\cdot\tilde{\boldsymbol{\tau}}_z^{-}]_{z_0} = 0. \tag{B3a}$$

This equation expresses that at $z = z_0$ the upgoing Green's functions do not 'interact' with the upgoing part of the wave field (waves that were reflected in the lower half-space $z > z_0$). Furthermore it can be verified that

$$[\tilde{\boldsymbol{\theta}}_{z,\Omega}^{\prime -}\cdot\tilde{\mathbf{U}}^{+} - \tilde{\mathbf{G}}_{\Omega}^{\prime -}\cdot\tilde{\boldsymbol{\tau}}_z^{+}]_{z_0} = \frac{2}{\rho\omega^2}\,]jk_{z,p}\tilde{\Gamma}_{\varphi,\Omega}^{\prime -}\tilde{\Phi}^{+} + jk_{z,s}\tilde{\mathbf{\Gamma}}_{\psi,\Omega}^{\prime -}\cdot\tilde{\mathbf{\Psi}}^{+}]_{z_0}. \tag{B3b}$$

Substitution of (B3a) and (B3b) into (B1a) yields

$$\Omega(\mathbf{r}_A, \omega) = \frac{2}{\rho\omega^2}\left(\frac{1}{2\pi}\right)^2 \iint_{-\infty}^{+\infty} [jk_{z,p}\tilde{\Gamma}_{\varphi,\Omega}^{\prime -}\tilde{\Phi}^{+} + jk_{z,s}\tilde{\mathbf{\Gamma}}_{\psi,\Omega}^{\prime -}\cdot\tilde{\mathbf{\Psi}}^{+}]_{z_0}\,\mathrm{d}k_x\,\mathrm{d}k_y. \tag{B4}$$

Substituting one-way wave equations (A7a) and (A7b) and applying Parseval's theorem again yields the one-way elastic Rayleigh integrals (19a) and (19b).

References

Aki, K. and Richards, P.G. 1980. *Quantitative Seismology.* W. H. Freeman and Co.

Berkhout, A.J. 1984. *Seismic Resolution: Resolving Power of Acoustic Echo Techniques.* Geophysical Press Ltd.

Berkhout, A.J. and Wapenaar, C.P.A. 1989. One-way versions of the Kirchhoff integral. *Geophysics* **54**, 460–467.

Berkhout, A.J. and Wapenaar, C.P.A. 1988. Delft philosophy on inversion of elastic data. 58th SEG meeting, Anaheim, Expanded Abstracts, 831–833.

Burridge, R. and Knopoff, L. 1964. Body force equivalents for seismic dislocations: *Bulletin of the Seismological Society of America*, **54**, 1875–1888.

De Hoop, A.T. 1958. Representation theorems for the displacement in an elastic solid and their application to elastodynamic diffraction theory. D.Sc. thesis, Delft University of Technology.

Dudgeon, D.E. and Mersereau, R.M. 1984. *Multidimensional Digital Signal Processing.* Prentice-Hall, Englewood Cliffs, N.J.

Kelly, K.R., Ward, R.W., Treitel, S. and Alford, R.M. 1976. Synthetic seismograms: a finite difference approach. *Geophysics* **41**, 2–27.

Kuo, J.T. and Dai, T.F. 1984. Kirchhoff elastic wave migration for the case of noncoincident source and receiver. *Geophysics* **49**, 1223–1238.

PAO, Y.H. and VARATHARAJULU, V. 1976. Huygens' principle, radiation conditions, and integral formulas for the scattering of elastic waves, *Journal of the Acoustical Society of America* **59**, 1361–1371.

PILANT, W.L. 1979. *Elastic Waves in the Earth.* Elsevier Science Publishing Co.

WAPENAAR, C.P.A. and BERKHOUT, A.J. 1989. Elastic wave field extrapolation. *Redatuming of Single- and Multi-component Seismic Data.* Elsevier Science Publishing Co.

WAPENAAR, C.P.A., HERRMANN, P., VERSCHUUR, D.J. and BERKHOUT, A.J. 1990. Decomposition of multi-component seismic data into primary P- and S-wave responses. *Geophysical Prospecting* (in press).

WAPENAAR, C.P.A., PEELS, G.L., BUDEJICKY, V. and BERKHOUT, A.J. 1989. Inverse extrapolation of primary seismic waves. *Geophysics* **54**, 853–863.